EarthArXiv Preprint Cover Sheet

Super El Niño Winters and the Arctic Polar Vortex: Response Heterogeneity, QBO Modulation, and a Prospectively Defined Test for Winter 2026/27

M. C. Tanyeri
Independent Researcher, Istanbul, Türkiye
ORCID 0009-0001-1575-5866 · mcantanyeri@outlook.com (corresponding author)

This manuscript is a non-peer-reviewed preprint submitted to EarthArXiv.

Peer-review status: this manuscript has not been peer reviewed. It has not yet been submitted to a peer-reviewed journal; submission to the Journal of Climate (American Meteorological Society) is planned. This is not a postprint, and no published version exists.

Version: 2 (6 September 2026). This version supersedes Version 1 (23 August 2026), which carried the title "The Super El Niño–Polar Vortex Paradox: QBO Modulation and a Testable Hypothesis for Winter 2026/27". The change of title reflects a change of framing after external critical reading; the numerical results are unchanged. A summary of the changes is given in the EarthArXiv version note.

Preprint DOI: https://doi.org/10.31223/X5MF74

Prospective test protocol (Appendix D): OSF project https://osf.io/bzg58 (formal registration pending). Reproducibility package: Zenodo DOI reservation pending; the archive will be linked here when published.

 Please cite as: Tanyeri, M. C., 2026: Super El Niño Winters and the Arctic Polar Vortex: Response Heterogeneity, QBO Modulation, and a Prospectively Defined Test for Winter 2026/27. EarthArXiv, Version 2, doi:10.31223/X5MF74.

Comments and criticism are welcome and should be sent to the corresponding author.

Super El Niño Winters and the Arctic Polar Vortex

Response Heterogeneity, QBO Modulation, and a Prospectively Defined Test for Winter 2026/27

M. C. TANYERİ
Independent Researcher, Istanbul, Türkiye
mcantanyeri@outlook.com
ORCID: 0009-0001-1575-5866
Corresponding author: M. C. Tanyeri, mcantanyeri@outlook.com

Abstract

In the three strongest El Niño winters of the instrumental record (1982/83, 1997/98, 2015/16) the Arctic polar vortex did not collapse in a major midwinter sudden stratospheric warming (SSW). This study starts from the premise that the observation is not a paradox: 58% of El Niño winters contain at least one major SSW, so the chance probability of three consecutive SSW-free winters is $0.42^3 \approx 0.07$, and the canonical El Niño signature in the literature is not an SSW but a vortex weakened on average in late winter. By that measure the three are not homogeneous: the DJF vortex of 1997/98 is below average (~21st percentile) and conforms to the canonical chain, 1982/83 is intermediate (~76th), and the true exception is 2015/16 (~97th), the winter in which the QBO was disrupted for the first time on record. We re-examine this heterogeneous record, on the occasion of the El Niño developing in 2026 with record-exceeding values forecast for October–December, using public index series (ONI, RONI, NAO, AO, QBO; 1951–2026), the NOAA SSW Compendium catalog (1958–2024) and ERA5 fields. Four results stand out. First, the intraseasonal sign asymmetry of the ENSO–NAO relationship (November–December r=+0.21, January–March r=−0.12) is an independent reproduction of published findings (Moron and Gouirand 2003; Ayarzagüena et al. 2018); our contribution is that the paired difference over the same winters excludes zero (Δr=+0.33; 95% CI +0.08/+0.56) and survives a moving-block bootstrap. Second, while the seasonal-mean surface trace of the QBO is near zero (QBO50×AO r=−0.01), the winter-based probability of an SSW appears higher in the easterly phase: the risk ratio is 1.26 (95% CI 0.75–2.12) under the pre-winter November 50-hPa definition and 1.48 (0.94–2.32) in the 67-winter 30-hPa record. Detecting a difference of this size with 80% power requires roughly 450 winters; the observational record cannot settle the question on its own, and a single winter moves the likelihood ratio by only ~1.2. In the continuous vortex regression ONI alone gives R^2=0.002 while adding wQBO raises R^2 to 0.126; this result rests on NCEP/NCAR Reanalysis-1. Third, the three winters defined by ONI≥+2.0 are westerly-QBO under the main phase definition (50 hPa, November), but the match is definition-dependent: at 30 hPa in DJF 1997/98 shifts to the easterly phase, and in 2015/16 the QBO was disrupted in February; the RONI≥+2.0 ruler enlarges the set to four with 1991/92 (4/4 SSW-free, 3/4 wQBO). The QBO is therefore not a deterministic switch but a possible conditioner of uncertain magnitude; the ONI–U10 relationship (r=−0.17) and the segmented fit (ΔAIC=−0.3) give no support to the vortex-level signature of a simple saturation scenario, and the mixed Central/Eastern Pacific structure of 2015/16 is added as a fourth candidate independent of the QBO. Fourth, the eastern Mediterranean end of the chain is measured directly with ERA5 (1979/80–2021/22, n=43): a +1 standard deviation stronger vortex is associated with a positive-NAM-like Z500 pattern in which 36.6% of grid cells in the Atlantic–European sector pass the BH-FDR (α=0.10) threshold and with a DJF precipitation anomaly of −5.5 mm month^{-1} [95% CI −10.2/−0.6] in the Türkiye box; a land-masked repetition preserves the DJF result, the fifteen regional coefficients do not pass BH-FDR as a single family, and the January–March link is erased when the NAO is controlled. The decision rules for 2026/27 (phase, event, ruler and evidence-updating criteria) are fixed in Appendix D before the outcome is known; the winter is not a verdict but a small Bayesian update of prospectively defined expectations.

Significance Statement

The intuition that "the warmer the Pacific, the harsher the European winter" is not a prediction rule supported by the record. That no major midwinter SSW occurred in the three strongest El Niño winters ever measured is striking at first sight; but because an SSW in an El Niño winter is roughly a coin toss, the trio is not by itself an anomaly demanding explanation, and the three winters do not resemble one another in vortex strength. The intraseasonal ENSO–NAO sign asymmetry is likewise not a new discovery but an independent reproduction of a published result. This study treats the QBO as one possible conditioner of this historical pattern: under the main phase definitions the probability of an SSW appears higher in easterly-QBO winters, but the effect size carries wide uncertainty. For Türkiye and the eastern Mediterranean, El Niño amplitude alone is not enough either; the chain that deserves more direct monitoring is vortex evolution, downward coupling, the NAO/AO and the Mediterranean circulation. In strong-vortex winters the large-scale Atlantic–European circulation tilts toward relatively suppressing the southerly storm track that brings precipitation to the Mediterranean; under a weak vortex the sign reverses. This revision measures that link with regional confidence intervals for the first time: the sign of the signal is consistent, its magnitude modest, and the individual regional intervals fragile under multiple-comparison correction — a picture that supports neither a deterministic reading nor outright dismissal. The scientific value of 2026/27 is not to prove or refute a hypothesis in a single winter, but to show how conditional expectations written before the outcome should be updated in the face of a new extreme event.

1. Introduction

As the summer of 2026 draws to a close, the equatorial Pacific is host to one of the most rapidly developing warm events of the instrumental era. The monthly Niño-3.4 anomaly reached +2.03 °C in July and the weekly value centered on 12 August reached +2.7 °C, with subsurface heat content at 50–150 m locally exceeding +8 °C. NOAA CPC assigns a probability above 90% to the "very strong" category for autumn and winter; in the RONI measure adopted as its official index in February 2026, which removes tropical-mean warming, the October–December median forecast of +2.66 °C exceeds every event since 1950. The question is no longer whether the event will occur, but how the global teleconnection network and the Northern Hemisphere stratosphere in particular will respond to forcing of this amplitude.

The canonical chain is well known. Strengthened convection in the central-eastern Pacific triggers a planetary-scale Rossby wave train that deepens the Aleutian Low. This deepening interferes constructively with climatological stationary wave-1, the largest-scale geographically anchored wave pattern of the atmosphere, and increases the upward wave activity directed into the stratosphere. When such waves reach the stratosphere they transfer momentum to the westerly circulation around the pole and can decelerate it; this planetary-wave forcing weakens the polar vortex (PV) (Bell et al. 2009; Cagnazzo and Manzini 2009). The full chain is sketched in Figure 1.

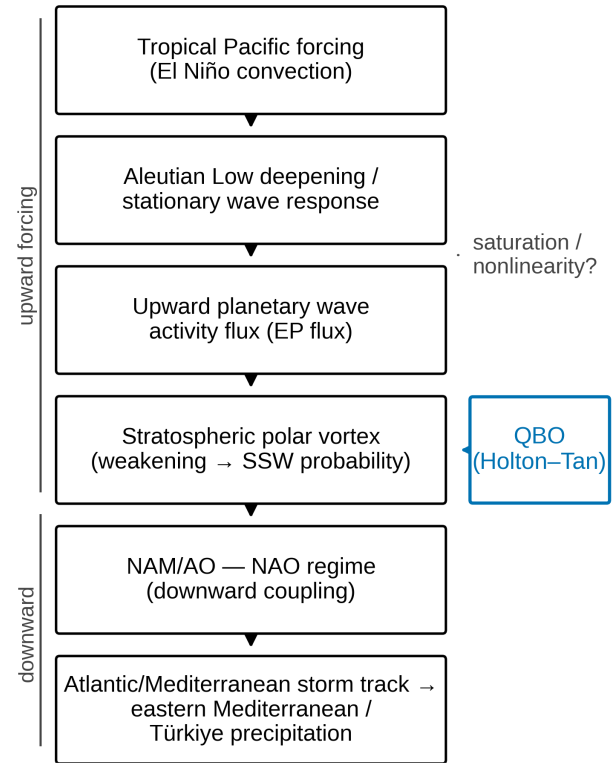

Figure 1. The canonical construction of the ENSO–stratosphere–Europe chain. The upward branch, running from tropical Pacific forcing to the Aleutian Low response and from there to the upward planetary wave activity flux and to vortex weakening / SSW probability, is drawn separately from the downward branch that descends through the NAM/AO–NAO regime to the Mediterranean storm track. Planetary waves carried along the upward branch transfer momentum to the westerly flow around the pole when they reach the stratosphere and can decelerate the vortex; the wave-activity box in the schematic represents this forcing. The box on the right marks the remote conditioning role of the QBO (Holton–Tan) acting on the vortex node, and the note on the left marks the saturation/nonlinearity question at the amplitude end of the forcing–response relationship. This is a conceptual schematic: it is not a composite map produced from numerical fields and cannot be used for quantitative interpretation (section 2.3).

If the weakening culminates in a major sudden stratospheric warming (SSW), a negative NAM/AO (Northern Annular Mode / Arctic Oscillation) signature descends into the troposphere over the following weeks (Baldwin and Dunkerton 2001), shifting the Atlantic storm track southward and increasing Mediterranean precipitation (Ineson and Scaife 2009; Domeisen et al. 2019; Zhang et al. 2024). The last link carries direct hydroclimatic significance for Türkiye: the strong negative relationship between winter precipitation and the NAO, especially for western Anatolia and Marmara, is among the most robust findings of the national literature (Türkeş and Erlat 2003, 2008; Baltacı et al. 2018).

Two remote controls recur throughout this chain. The Quasi-Biennial Oscillation (QBO) is the oscillation of equatorial stratospheric winds between westerly (wQBO) and easterly (eQBO) phases with a mean period of about 28 months, and it remotely tunes the receptivity of the vortex to planetary waves arriving from below. The North Atlantic

Oscillation (NAO) and the closely related Arctic Oscillation (AO) are the leading modes of Atlantic–European variability and set the latitude of the storm track: storms are directed toward northern Europe in the positive phase and toward the Mediterranean in the negative phase.

Findings that strain the textbook narrative have nevertheless accumulated at every link. SSW frequency does not increase in a way specific to El Niño but rises in both ENSO phases (Butler and Polvani 2011); Garfinkel et al. (2012a) attribute this to the relative insulation from the ENSO teleconnection of the North Pacific region where SSW precursors are most sensitive, and Palmeiro et al. (2023) show that the significance of the phase difference disappears in the 1950–2021 ERA5 record. It matters here that the canonical ENSO signature reported in the literature is not an SSW at all but a late-winter mean state — a warmed polar stratosphere and a weakened vortex around February (Manzini et al. 2006; Cagnazzo and Manzini 2009; Ineson and Scaife 2009) — so the absence of a binary event label does not by itself place a winter outside the canonical chain. Second, the assumption that the stratospheric response grows linearly with forcing shows signs of saturation for extreme events: Toniazzo and Scaife (2006) and Hardiman et al. (2019) find the North Atlantic response to the very strongest events different from that to moderate ones and carried largely by the tropospheric pathway, Trascasa-Castro et al. (2019) test the linearity of the stratospheric and Euro-Atlantic response across ENSO amplitudes, Jiménez-Esteve and Domeisen (2020) show the tropospheric pathway itself to be nonlinear, Rao and Ren (2016a,b) document the asymmetry of the stratospheric response in observations and in WACCM, and Zhou et al. (2019) and Manzini et al. (2024) disagree on whether the El Niño branch saturates. A candidate independent of amplitude is event flavor: central-Pacific events force the vortex differently from eastern-Pacific ones and need not weaken it (Garfinkel et al. 2013; Hegyi et al. 2014; Iza and Calvo 2015), which bears on the mixed structure of 2015/16. Third, the Holton–Tan effect (Holton and Tan 1980; Anstey and Shepherd 2014) weakens the vortex under easterly QBO, but reportedly loses strength in El Niño winters (Wei et al. 2007; Garfinkel and Hartmann 2008; Calvo et al. 2009; Kumar et al. 2022). Fourth, the claim that SSW morphology differentiates the surface signature is supported in reanalysis composites (Mitchell et al. 2013; Seviour et al. 2013; Hall et al. 2021) but dissolves beyond the first weeks in large model ensembles (Maycock and Hitchcock 2015; White et al. 2019, 2021; Lehtonen and Karpechko 2016).

How anomalous the three super winters are depends on the measure applied to them, and the framing adopted here differs from the one that motivated the earlier version of this work. On the binary SSW label the coincidence is real but weak: 58% of El Niño winters in the catalog contain at least one major event (section 3), so three SSW-free winters in succession carry a base-rate probability near $0.42^3 \approx 0.07$ — close to the permutation reference derived independently in section 5, and not in itself a strong signal that something requires explanation. On the continuous measure the three are not a homogeneous set at all: the DJF 10-hPa 60°N zonal-mean wind places 2015/16 near the top of the record (97th percentile), 1982/83 above average (76th) and 1997/98 below average (21st). Read against the canonical late-winter signature rather than the binary label, 1997/98 belongs with the textbook chain, 1982/83 is intermediate, and only 2015/16 — the winter in which the QBO was disrupted for the first time in the observational record (Osprey et al. 2016; Newman et al. 2016) — stands out as a clear exception. The object of study is therefore not a paradox but a graded heterogeneity, and the question is how much of it a background condition such as the QBO can account for.

This study combines these lines of debate in a single framework, through the 2026/27 case and from an eastern Mediterranean perspective. Published coefficients and composites are compiled with source verification, while the relationships that form the backbone of the claims are recomputed independently from publicly available series. Five questions are addressed: (i) to what extent is the intraseasonal structure of the ENSO–NAO relationship — an established result that is reproduced rather than discovered here (section 3) — lost in single-season means, and can the contrast be given an interval rather than a sign; (ii) does the Holton–Tan effect live as a surface correlation or as a modulator of event probability, and how robust is that reading to the phase definition and to the power available; (iii) how much of the SSW-free character of super El Niño winters can be attributed to the QBO phase once the base rate and the vortex-level heterogeneity are accounted for; (iv) does the saturation claim survive a continuous vortex measure rather than a binary SSW label; and (v) how large is the observational link between vortex strength and the European–Mediterranean circulation and Turkish winter climate when measured directly with grid-level FDR control and regional confidence intervals? Our search did not identify a direct, quantitative, station-scale literature linking vortex state to Turkish precipitation; as a first step we compute that link at the reanalysis scale (section 7.1) and leave station-scale verification as future work. Section 2 presents data and methods; sections 3–7 treat the ENSO–vortex pathway, the two faces of Holton–Tan, QBO×ENSO interference, SSW typology and the European–Turkish teleconnections; section 8 the 2026/27 case and the prospectively defined protocol fixed in Appendix D; section 9 discusses the results, the limits of sample power and the follow-up design built on large-ensemble hindcasts; and section 10 states the conclusions.

2. Data and Methods

2.1 Data

For the ENSO state we use the ERSSTv6-based ONI series of NOAA CPC (product: Seasonal ERSSTv6, centered base periods; file `oni.ascii.txt`; 1950–MJJ 2026) and the complementary RONI series from the same product family (Seasonal Relative ERSSTv6, 1991–2020 base period; file `RONI.ascii.txt`), both downloaded on 28 August 2026 and archived in the reproduction repository. Because peak ONI values can differ between ERSST versions, the three-winter set defined by the ≥+2.0 threshold is specific to the ERSSTv6 ruler; Appendix A and the parallel RONI reporting test that dependence explicitly. For the NAO and AO we use the monthly CPC indices (1950–July 2026), which are the rotated-EOF and 1000-hPa height-EOF definitions and can differ from station-based alternatives (Hurrell; Gibraltar–Iceland) by ±0.05–0.1 in correlation. Two series are used for the QBO: the 50-hPa equatorial zonal-mean wind (NOAA CPC/CDAS, 1979–July 2026) and the 30-hPa equatorial zonal-mean wind (NOAA PSL, 1948–2026). Their zonal-mean nature reduces amplitudes relative to Singapore station data (FUB/NASA) and can shift phase transitions by about one month; because our findings rest on the sign of the phase this does not affect them qualitatively, but it is taken into account for the 2026/27 phase timing in section 8. The access date for all index series is 28 August 2026 and the product identification is repeated in every table and figure caption.

SSW events are taken from the NOAA CSL SSW Compendium (within the framework of Butler et al. 2015, 2017): a major SSW is defined by the reversal to easterlies of the 10-hPa, 60°N zonal-mean zonal wind during November–March (Charlton and Polvani 2007); central dates are taken with ERA5 priority and, for events absent from ERA5, from the JRA-55 and NCEP/NCAR columns. Because the Compendium ends in 2023, the events of 16 January and 4 March 2024 were added following Lee (2025) and are flagged explicitly in the tables. The Compendium's own ENSO and QBO labels are nowhere used in this study; all conditioning variables are derived from independent series (see section 2.2). The split/displacement classification is method-dependent — the zonal-mean criterion of Charlton and Polvani (2007) and the two-dimensional moment diagnostic of Mitchell et al. (2013) can assign different types for an appreciable fraction of borderline cases (for classification uncertainties see Baldwin et al. 2021) — so a type is assigned only to recent events for which there is broad agreement in the literature, with disputed cases marked by an asterisk. Vortex strength is computed as the DJF mean of the 10-hPa, 60°N zonal-mean zonal wind from NCEP/NCAR Reanalysis-1 (Kalnay et al. 1996; NOAA PSL THREDDS subsetting service; stratospheric values before 1958 should be read with caution). ERA5, whose record has been extended back to 1940, and JRA-3Q are better products for this quantity; Reanalysis-1 is retained here only because the reproduction chain was built on it, and re-deriving the U10–60N series from ERA5 (1940–2026) so that Table 1, Table 2a and Figure 7 are repeated with that product is recorded as a predefined step to be completed before journal submission (Appendix D). Unless stated otherwise, the 10-hPa coefficients in this study are Reanalysis-1 values.

Monthly ERA5 fields are used for the regional analysis (section 7.1) (Hersbach et al. 2020): 500-hPa geopotential height (Z500, m), total precipitation (mm $month^{-1}$) and 2-m temperature (K) are derived from the 1.5°, conservatively regridded ERA5 product in the WeatherBench2 archive (Rasp et al. 2024). Z500 and 2-m temperature are monthly means of 6-hourly steps; for precipitation, the 6-hourly accumulations of the WeatherBench2 variable total_precipitation_6hr were summed over each month and converted from meters of water equivalent to millimeters using a factor of 1000, giving monthly accumulated precipitation (mm $month^{-1}$). The extracted window is November 1978–December 2022 and the domain is 80°W–50°E, 20–80°N; the access date is 29 August 2026. Coastlines are Natural Earth 50 m.

2.2 Definitions and statistics

"Winter Y" denotes the period from December of Y−1 through February of Y. The ENSO phase is defined by ONI_DJF (El Niño ≥ +0.5 °C, La Niña ≤ −0.5 °C); the operational "super" category of this study is ONI_DJF ≥ +2.0 °C, and the entire historical classification rests on that single measure. RONI, which removes tropical-mean warming, serves only as a complementary sensitivity ruler and as a characterization of the current 2026/27 context; the two indices are nowhere operated as interchangeable versions of the same threshold system. The effect of the threshold choice (≥+1.5, ≥+1.8, ≥+2.0) on the main pattern is presented in Appendix A (Table A1), and the catalog is additionally constructed with the RONI ruler (Table A2).

The QBO phase is defined with a pre-winter window so that the conditioning variable does not overlap the outcome period: the main classification is the sign of the November mean of the 50-hPa equatorial zonal-mean wind, with November–December and December–February classifications reported as sensitivity analyses. In 41 of the 45 winters between 1980 and 2024 (91%) the November and DJF labels agree, the four exceptions being transition winters (1983/84, 1986/87, 1992/93, 2017/18), and the November and November–December labels agree in 100% of cases. Taking seriously the warning that a single level may be insufficient (Dunkerton et al. 1988; Gray et al. 2018), the entire classification was repeated at 30 hPa, where the November labels of the two levels agree in 35 of the 45 winters; pre-1979 phase labels come from the 30-hPa series alone. All QBO labels are derived from the wind series alone, independently of the SSW catalog. The continuous vortex analysis has two layers: the correlation and segmented fit use the full 1959–2024 record (n=66), whereas the regression including the QBO is fitted by ordinary least squares to the joint sample with ONI, U10–60N and the November 50-hPa phase all available (n=45, 1980–2024). The nested models are U10 ~ ONI; U10 ~ ONI + wQBO; and U10 ~ ONI + wQBO + ONI×wQBO, compared using R^2, adjusted R^2 and AIC.

Early winter is represented by November–December and late winter by January–March; this division is taken from the two-pathway literature (Ineson and Scaife 2009; Bell et al. 2009) and was not optimized against the data, nor was it prospectively specified. The framework is entirely exploratory: p values are descriptive measures accompanying effect sizes and confidence intervals rather than confirmatory thresholds, and no multiple-comparison correction is applied in the index-layer analyses. Correlations are Pearson coefficients with Fisher-z transformed 95% intervals; the early/late-winter difference is bounded by a paired bootstrap over the same winters (20 000 replicates) and repeated with a moving block bootstrap (L=3, 5, 8) to guard against serial dependence. For winter-based SSW rates the outcome is always the binary "at least one major event within the winter"; cell uncertainties are Clopper–Pearson exact intervals, the phase difference is expressed as a risk ratio with Fisher's exact test, and the ENSO×QBO interaction uses Firth penalized logistic regression with a profile penalized likelihood ratio test. For the super El Niño–wQBO coincidence the reference probability is computed with two randomizations preserving the actual historical QBO phase sequence (circular shifting and three-winter block permutation); the naive value of 0.125, which assumes independence and equal phase frequency, is mentioned only for comparison. The assessment of the Türkiye-scale literature rests not on a systematic search protocol but on the peer-reviewed sources accessible to the author, and statements of absence are calibrated accordingly.

The regional ERA5 regression (section 7.1) covers the winters 1979/80–2021/22 (n=43), with anomalies relative to the 1991–2020 climatology. The predictor is the standardized DJF U10–60N (NCEP R1; section 2.1), and the response fields were regressed separately in the DJF, November–December (ND) and January–March (JFM) windows. Coefficient uncertainties are 95% percentile intervals from a winter-based bootstrap (B=5000; fixed seed); multiple comparisons over the grid are addressed with the Benjamini–Hochberg false discovery rate approach, and for the maps only the fraction of cells passing BH-FDR (α=0.10) is reported (Benjamini and Hochberg 1995; Wilks 2016) — a descriptive fraction, not a field-significance test. Regional effects are area means over five boxes defined geographically without reference to the data: the Türkiye box (26–45°E, 36–42°N; 65 cells), Marmara (26–30.5°E, 39.5–42°N; 6 cells), the Aegean (26–30.5°E, 36.5–39.5°N; 6 cells), the Mediterranean coast (29.5–36.5°E, 36–37.5°N; 10 cells) and the eastern Mediterranean/Levant (25–37°E, 31–37°N; 32 cells). In all five the average is a cosine-latitude-weighted full-area mean: no land–sea mask is applied and ocean cells are included, a description corrected during the reproducibility audit without any numerical result changing. At 1.5° resolution these averages are coarse, and the "Türkiye box" is a reanalysis box-area mean rather than a Türkiye average in the administrative sense. The role of the NAO is assessed by comparing Model A (regional precipitation ~ U10s) with Model B (~ U10s + NAO) and by the bootstrap interval of the indirect component; this is an observational decomposition, not evidence of causal mediation. Regressing the ND window on the DJF predictor is partly acausal, so each window was repeated with its own concurrent predictor and the beta-map pattern correlations are reported (DJF 1.00, JFM 0.96, ND 0.68). Coefficients are per +1 standard deviation of U10 (strong vortex), with signs reversed for the weak-vortex reading. Three windows × five regions form a single exploratory family of fifteen coefficients; under BH-FDR (α=0.10) none passes the threshold (smallest p=0.022). The sensitivity of the box means to sea cells is reported in Table C3, where the same five boxes are repeated as land-cell means restricted by the ERA5 land–sea mask (land fraction ≥0.5); at 1.5° the Marmara box shrinks to four cells under the mask, and this repetition does not substitute for station-scale verification. A 0–60-day lagged design and station-scale verification (MGM long series, E-OBS) were deliberately left outside this revision as future work. Reporting many QBO definitions, three ONI thresholds and three seasonal windows together is a sensitivity ladder, but it is also a map of forking analysis paths; for that reason the level, month, SSW definition and ENSO ruler that will count for 2026/27 are fixed as a single rule set in Appendix D, to be deposited in a timestamped registry (OSF) before submission.

2.3 A note on the figures

Figures 1–6 are conceptual schematics: they are not composite maps produced from numerical fields but script-drawn vector diagrams that convey the qualitative pattern of the data described in section 2.1 and of the cited literature composites (coastlines: Natural Earth 50 m). They cannot be used for quantitative interpretation, and this limitation is repeated in every caption. Figures 7–9 and Figure C1 are the exception to that rule: they are quantitative figures produced directly from the series and fields of section 2.1, and their captions give the data identification and the access date.

3. The ENSO–Vortex Pathway: Intraseasonal Structure and the Saturation Question

The first test of the canonical chain is whether the ENSO signature at the Atlantic end appears in a simple seasonal mean. Over 1951–2026 the correlation between ONI(DJF) and NAO(DJF) is −0.04 (Table 2a, row 1). Divided into intraseasonal windows, r=+0.21 in early winter (November–December; 95% CI −0.01/+0.42; p=0.06) and r=−0.12 in late winter (January–March; 95% CI −0.33/+0.11); both are weak and their intervals include zero. By contrast, a paired bootstrap over the same winters gives Δr=+0.33 (95% CI +0.08/+0.56) for the difference between the windows, preserved under the moving block bootstrap (+0.09/+0.54 for L=3, +0.11/+0.53 for L=5, +0.13/+0.54 for L=8). What is strong is not the individual correlations but the systematic differentiation between the windows, and a single DJF mean can render the ENSO–NAO relationship invisible by adding together opposing intraseasonal tendencies.

This intraseasonal structure is an established result and is not claimed as a new one. Moron and Gouirand (2003) documented the seasonal modulation of the ENSO–North Atlantic sea level pressure relationship over 1873–1996; Ayarzagüena et al. (2018) established the same early-winter/late-winter contrast in both observations and models; King et al. (2018) showed that the late-autumn teleconnection operates through a mechanism distinct from the late-winter one; and Mezzina et al. (2020) analyzed the late-winter dynamics in detail. What is offered here is independent reproduction from public series together with a measurement choice: the contrast is expressed as a paired-bootstrap difference between windows computed over the same winters, with an interval attached, rather than as an informal comparison of two separately estimated correlations. Reproducibility of this kind carries its own value, and it is on that basis rather than on novelty that the result is presented.

Composites show the same structure at the event level. Across twenty-five El Niño winters the NAO falls from a November–December mean of +0.33 to +0.02 in January–March; restricted to strong events (ONI ≥ +1.5; n=7) the decline runs from +0.69 to +0.29 and the late-winter AO mean reaches −0.28. An important qualification is that the composite shows a weakening rather than a full sign reversal. The reversal is event-dependent, with clear examples — from +0.42 to −1.19 in 1957/58, from +1.64 to −0.58 in 1986/87 and from +0.77 to −0.34 in 1979/80 — while 2015/16 spent the entire winter on the positive side (+1.99 → +0.81). Geng et al. (2017) show that the abrupt early-January reversal in super events can arise, independently of the stratosphere, from the interaction of the event with the annual cycle of the subtropical jet; the spread in our composite implies that this mechanism does not operate with the same strength in every event (Figure 2).

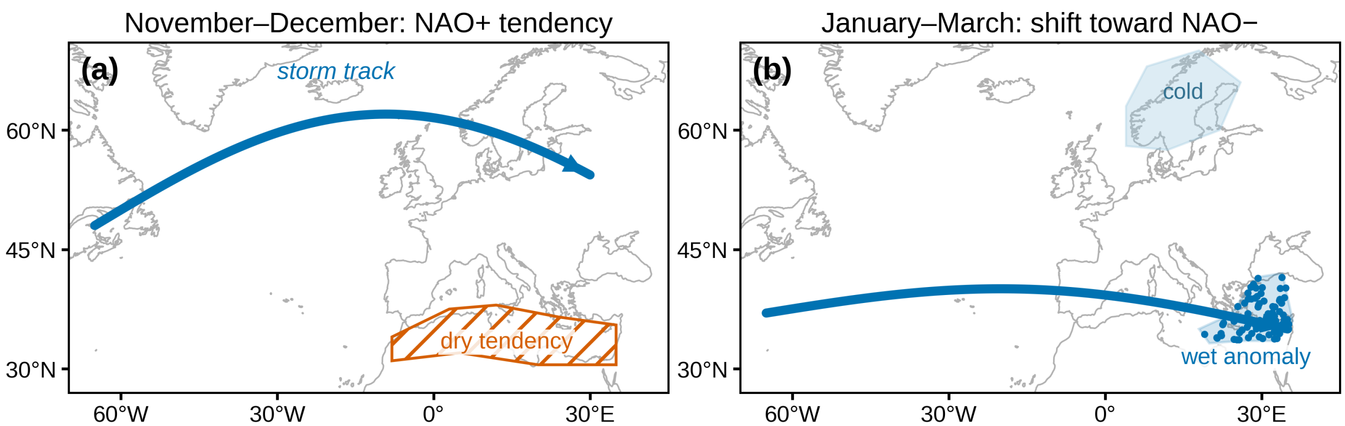

Figure 2. Intraseasonal sign asymmetry of the North Atlantic response in El Niño winters. (a) November–December: a tendency toward NAO+, a northward-shifted storm track and a dry-signed anomaly over the Mediterranean. (b) January–March: a shift toward NAO−, a southward-displaced flow, wet-signed anomalies over the eastern Mediterranean and cold-signed anomalies over northern Europe. The patterns are a qualitative summary of the correlations reported in section 3 and of the cited literature composites. This is a conceptual schematic: it is not a composite map produced from numerical fields and cannot be used for quantitative interpretation (section 2.3).

SSW frequency is the second test. In the 1958–2024 record there are 7.9 major SSWs per 10 phase-winters in El Niño winters, 7.4 in La Niña winters and 5.5 in neutral winters; these are descriptive event densities scaled by the number of phase-winters, not rates per chronological decade. On a winter basis the fractions with at least one major SSW are 58%, 65% and 45% (Table 3a). Both ENSO phases exceed neutral winters while the El Niño–La Niña difference is small. Read together with Butler and Polvani (2011) and the longer-record analysis of Palmeiro et al. (2023), which finds no discriminating difference between phases, this underlines the sensitivity to period and classification; our numbers are consistent with the phase-symmetry explanation of Garfinkel et al. (2012a). The 58% figure also fixes the reference against which the super-winter coincidence must be judged: if an El Niño winter contains a major SSW with probability near 0.58, then three successive SSW-free winters arise with probability near $0.42^3 \approx 0.07$ with no mechanism invoked at all.

The weakest link is the amplitude assumption, but the evidence it has to explain is thinner than it first appears. In the three winters with the largest forcing — 1982/83, 1997/98 and 2015/16, the peaks of the catalog (Table 1) — there is no major midwinter SSW, yet the vortex strengths differ by more than 25 m s^{-1} and only 2015/16 sits at record strength (Ren et al. 2017). Zhou et al. (2019) offer a physical candidate for saturation: in extreme events the westward expansion of convection toward the Maritime Continent disrupts the constructive interference of the anomalous wave train with climatological wave-1, so the forcing grows while its effective projection does not. Toniazzo and Scaife (2006) and Hardiman et al. (2019) reach a related conclusion from the Atlantic end, attributing the response of the strongest events largely to the tropospheric pathway, whereas Trascasa-Castro et al. (2019) find the stratospheric and Euro-Atlantic response broadly linear in amplitude and Manzini et al. (2024) report that the El Niño branch remains approximately linear in the model world. A fourth possibility bypasses amplitude altogether: the vortex response depends on where in the Pacific the warming sits, and central-Pacific events need not weaken the vortex (Garfinkel et al. 2013; Hegyi et al. 2014; Iza and Calvo 2015), which is directly relevant to the mixed eastern/central-Pacific structure of 2015/16. This debate is taken up with a continuous vortex measure at the end of section 5, which also brings in the QBO phase.

4. The Two Faces of Holton–Tan: A Dead Correlation and a Live Probability

The stratospheric body of the Holton–Tan effect is not in dispute: in easterly-QBO winters the vortex is weaker than under westerly QBO by more than 10 m s^{-1} at 10 hPa (Holton and Tan 1980; Anstey and Shepherd 2014; Watson and Gray 2014). The relationship is strongest when defined near 50 hPa — Watson and Gray (2014) justify that level by the correlation of 0.58 between the November–February equatorial wind and the 60°N/10-hPa wind — whereas Dunkerton et al. (1988) and Gray et al. (2018) argue that the deep phase profile rather than a single level is decisive. On the mechanism side the classical zero-wind-line/waveguide account competes with the secondary meridional circulation of the QBO, and idealized experiments favor the latter (Garfinkel et al. 2012b; Watson and Gray 2014). The effect is also known to be strong in early winter and to weaken, or change sign, in late winter (Lu et al. 2020). Figure 3 shows the opposing effects of the two phases on the waveguide.

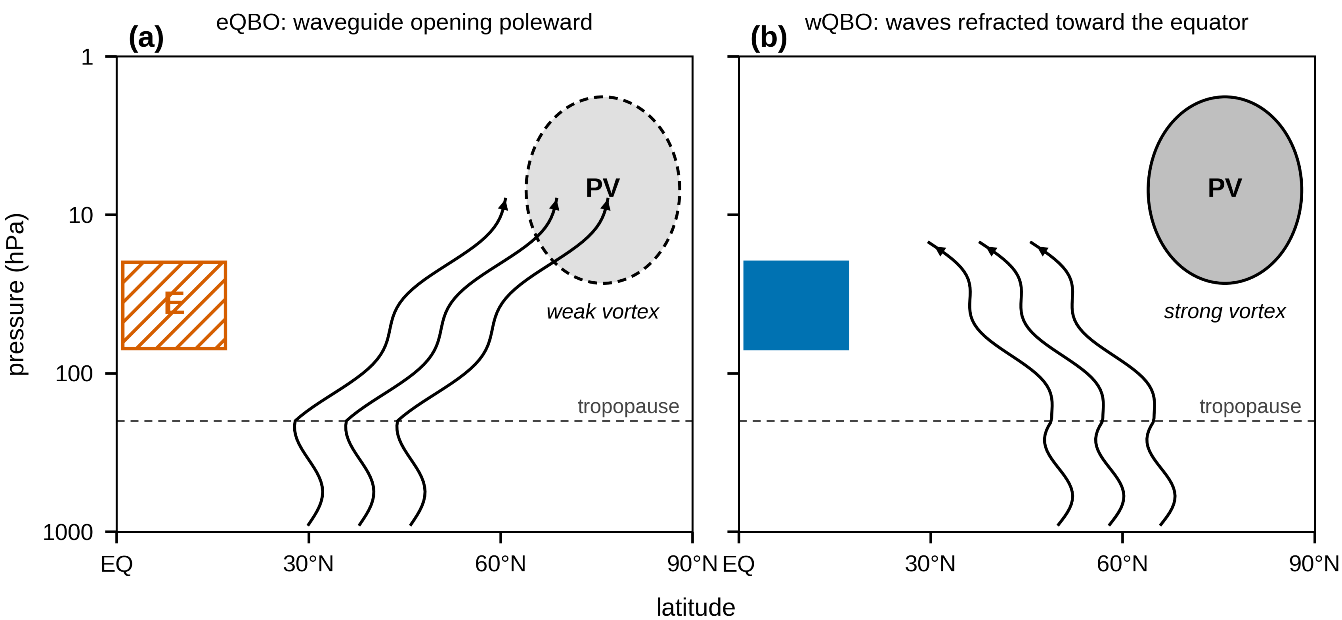

Figure 3. The waveguide interpretation of the Holton–Tan mechanism. (a) Under easterly QBO the equatorial easterly layer forms a critical line that directs planetary waves poleward and leaves the vortex more exposed to wave forcing. (b) Under westerly QBO the waves refract toward the equator and the vortex is relatively protected. The pressure axis is logarithmic; PV denotes the polar vortex and the dashed outline a weakened vortex. This is a conceptual schematic: it is not a composite map produced from numerical fields and cannot be used for quantitative interpretation (section 2.3).

At the surface, by contrast, the effect either disappears or becomes apparent depending on the measurement language, and that duality is the second main finding of this paper. In the language of seasonal-mean correlation there is no trace: r=−0.01 between QBO50(November–December) and AO(DJF) (n=47), and +0.06 for QBO30 (n=76); the phase composites are likewise not discriminating (AO mean −0.03 in the W phase and −0.01 in the E phase; Table 2a, rows 6–8).

In the language of events the trace becomes visible, but its precision is sensitive to the phase definition. Under the pre-winter definition adopted here as the main one (November 50 hPa; 1980–2024), 63% of easterly-QBO winters see at least one major SSW against 50% of westerly-QBO winters (12/19 versus 13/26); the risk ratio is 1.26 (95% CI 0.75–2.12; Fisher's exact test p=0.545). The single continuous series that extends the sample to 67 winters (30 hPa, 1958–2024) gives 67% versus 45%, risk ratio 1.48 (0.94–2.32; p=0.089). A definition built on the DJF mean raises the ratio further (1.71; 0.99–2.96), but because it overlaps the conditioning variable with the outcome period it is reported only as an upper bound in Table 3b and Figure 8a and is not used in any inference. The definitions share the constancy of the direction; their common weakness is that the confidence intervals include unity. Holton–Tan therefore reaches the surface not as a seasonal-mean correlation but as a shift in event probability of order 1.3–1.5 that cannot be pinned down with the present sample.

The real limit is sample power. To detect a difference between proportions of 63% and 50% (a risk ratio of 1.26) at two-sided α=0.05 with 80% power requires roughly 230 independent winters per group, about 450 in total; the 45-winter record cannot settle this question on its own, and each new winter, through the likelihood ratio derived from the cell proportions of Table 3b, can shift the weight given to Holton–Tan conditioning by a factor of only about 1.2 (Appendix D). This does not diminish the value of the prospective record; it requires saying at the outset that no single winter will be a verdict.

The contradiction between the two languages is only apparent, and its resolution lies in the sparseness of stratosphere–troposphere coupling: only about half of SSWs bring the canonical negative-NAM signature down to the surface (Karpechko et al. 2017; Baldwin et al. 2021), and once that signal is diluted in the same seasonal mean by the events that do not descend and by SSW-free winters, the correlation evaporates. The reading is consistent with the composite-based surface signature of Marshall and Scaife (2009) and with the QBO being a genuine source of skill in ensemble-mean seasonal forecasting (Scaife et al. 2014; the Atlantic imprint known since Ebdon 1975): predictability comes from the distillation of a probability shift within an ensemble, not from the raw index correlation.

5. QBO × ENSO Interference and the Super El Niño–wQBO Coincidence

When the two modulators are superposed the interaction is not linear. The observational and modeling literature converges on the finding that the Holton–Tan modulation remains strong in La Niña winters and weak in El Niño winters (Wei et al. 2007; Garfinkel and Hartmann 2008; Calvo et al. 2009; Richter et al. 2011); Kumar et al. (2022) further strain pure additivity by showing that westerly QBO and El Niño can interfere constructively over the Aleutian Low.

The present analysis can neither confirm nor exclude that picture. With the pre-winter November 50-hPa phase over 1980–2024 (Table 3c), the eQBO and wQBO cells give the same fraction in El Niño winters (3/6 and 5/10; both 0.50). The difference appears larger in neutral winters (4/7 versus 1/6), but the cells are limited to six or seven winters. Using the 30-hPa November phase and the 67-winter record, the El Niño cells separate again (eQBO 9/13=0.69; wQBO 5/11=0.45). In the Firth penalized logistic model the interaction term has an odds ratio of 0.47 in the short record (95% CI 0.04–5.96; $p=0.541$) and 1.13 in the long record (0.14–8.92; $p=0.904$). Because the point estimates change with the definition and the intervals are wide, neither the direction nor the magnitude of the ENSO×QBO interaction can be resolved with the present sample.

The continuous vortex measure provides different information, but it does not measure the saturation mechanism itself. Across the 66 winters between 1959 and 2024 the relationship between ONI and the DJF mean U10–60N is weak and consistent with zero ($r=-0.17$; $p=0.16$; slope -1.6 m s^{-1} °C^{-1}); for RONI, $r=-0.16$. Although the best break in the segmented fit is found at +1.6 °C, model selection does not support a break (ΔAIC=−0.3; Figure 7). This provides no observational support for the continuous signature expected at the vortex level under a simple saturation scenario, and it is not a direct test of the proposed convection → wave-1 interference → upward wave flux mechanism. The three super winters fall at the 21st, 76th and 97th percentiles of the U10 distribution and are therefore not homogeneous. In the joint sample (n=45; 1980–2024) the ONI-only model gives $R^2=0.002$ (adjusted $R^2=-0.02$; ONI coefficient −0.37 m s^{-1} °C^{-1}, 95% CI −3.14/+2.40, $p=0.79$). Adding the wQBO indicator raises R^2 to 0.126 (adjusted $R^2=0.085$; ΔAIC=−4.0), with wQBO associated with a vortex stronger by +6.79 m s^{-1} (95% CI +1.19/+12.39; $p=0.019$). The ENSO×QBO term adds only 0.005 to R^2, has a coefficient of −1.25 m s^{-1} °C^{-1} (95% CI −6.83/+4.33; $p=0.65$) and worsens the AIC (ΔAIC=+1.8). The QBO here is not a deterministic switch but a conditioner more visible than ENSO amplitude in this sample and yet limited. The regression rests on NCEP/NCAR Reanalysis-1, which is a limitation of the present version and not a necessity: ERA5 now extends back to 1940 (Hersbach et al. 2020; Soci et al. 2024) and JRA-3Q to 1947 (Kosaka et al. 2024), both freely available after registration, and the U10–60N series is being rebuilt from ERA5 so that the product dependence of the coefficients reported here can be assessed (section 9).

On this basis the most prominent pattern in the catalog should be read with the distinction between evidence and pattern preserved, and with the heterogeneity of section 1 kept in view. All three winters with ONI≥+2.0 — 1982/83, 1997/98 and 2015/16 — coincided with wQBO conditions and none experienced a major midwinter SSW, whereas the strong, easterly-QBO winter of 2023/24 produced two major SSWs (Table 1; Lee 2025). But the binary label conceals a spread of more than 25 m s^{-1} in vortex strength, the base rate of section 3 makes a run of three SSW-free winters a roughly one-in-fourteen outcome without any mechanism, and n=3 cannot turn the correspondence into a causal explanation or a forecasting rule. The defensible status is a hypothesis-generating observational pattern testable against new events.

The claim of QBO-phase robustness must be qualified at the level of definition. The three-of-three wQBO pattern is preserved under the 50-hPa November, 50-hPa November–December, 50-hPa DJF and 30-hPa November classifications, whereas under 30-hPa DJF 1997/98 shifts to the easterly phase (Table A3); given that the 50-hPa DJF window overlaps the outcome period, a statement of the form "robust under all QBO definitions" is not appropriate. The November 50-hPa wind is westerly but weak in the three super winters (+0.4, +1.2, +1.3 m s^{-1}), while the 30-hPa November values are more clearly westerly (+9.5, +5.7, +12.8 m s^{-1}). In randomizations preserving the actual 30-hPa phase sequence, the reference probability that all three fall in the westerly phase is 0.091 under circular shifting and 0.056 under three-winter block permutation; this 0.06–0.09 range suggests the pattern may not be entirely ordinary but does not exclude chance given the small sample.

The fragility of the pattern is evident in the threshold sensitivity and in the counterexamples. In the strong-but-not-super band, 1957/58 (ONI +1.7) produced an SSW under wQBO, while 1991/92 (+1.5) passed without an SSW under eQBO. Although the November and DJF means were westerly in 2015/16, the disruption of the QBO in February 2016 (Osprey et al. 2016; Newman et al. 2016; Coy et al. 2017; Barton and McCormack 2017) illustrates the physical limitation of a single-level classification. The wQBO phase is therefore neither a necessary nor a sufficient condition for the absence of an SSW. There is also an explanation for 2015/16 that looks outside the QBO: that event had a markedly mixed structure with a Central Pacific component (Paek et al. 2017), and Central-Pacific-weighted El Niños have been reported not to weaken the vortex, or even to strengthen it (Hegyi et al. 2014; Garfinkel et al. 2013; Iza and Calvo 2015); section 8.2 defines this possibility separately as a fourth candidate (H4).

Changing the ruler affects the two components of the pattern in opposite directions. Under ONI≥+2.0 the cluster comprises three winters and is 3/3 wQBO and 3/3 SSW-free. Under RONI≥+2.0, 1991/92 joins: all four winters are SSW-free, but only three are wQBO (Table A2). The SSW-free component thus strengthens in the transition from ONI to RONI while QBO-phase purity weakens, so the observational pattern and the wQBO explanation of it are not equally index-robust. The first genuine eQBO super El Niño will discriminate H2 more directly than the present 2026/27 configuration, whose expected wQBO pushes the conditional expectations of H1 and H2 largely in the same direction.

The continuous measure behind the binary "SSW-free" label reinforces that reading. Winter 2015/16 carries one of the strongest vortices in the record (44.4 m s⁻¹; ~97th percentile), 1982/83 is above average (36.6 m s⁻¹; ~76th) and 1997/98 is below average (19.6 m s⁻¹; ~21st percentile) — it produced no SSW, but neither did it carry a strong vortex (Table 1, U10–60N column). "The vortex does not break down in super winters" should therefore not be read as "the vortex is always strong": the common denominator is the absence of a reversal, not a common vortex state. Against the canonical late-winter expectation of a weakened vortex, 1997/98 is a conforming case and only 2015/16 departs clearly — and 2015/16 is also the winter in which the QBO was disrupted, which makes it a poor witness for a clean QBO-phase argument. The continuous measure is carried forward to section 8.3 and Appendix D as a richer test variable than the binary label.

What the observational record cannot do should be stated plainly at this point. The ENSO×QBO cells hold between six and thirteen winters, and even the marginal QBO contrast rests on 45; a risk ratio of the order estimated in section 4 cannot be resolved on such a sample, and no plausible extension of the observational record within a working lifetime will resolve it. The route that can is a large initialized ensemble. The ECMWF SEAS5 hindcast set (1981–2016, 51 members; Johnson et al. 2019) supplies of order 1,800 model winters started from observed ENSO and QBO states, so that the ENSO×QBO cells are populated by hundreds rather than tens of winters, and the multi-system C3S archive multiplies that further. Such a design lies beyond the scope of the present observational study; it is identified here as its natural continuation, and the limitations recorded in section 9 should be read as the specification for it.

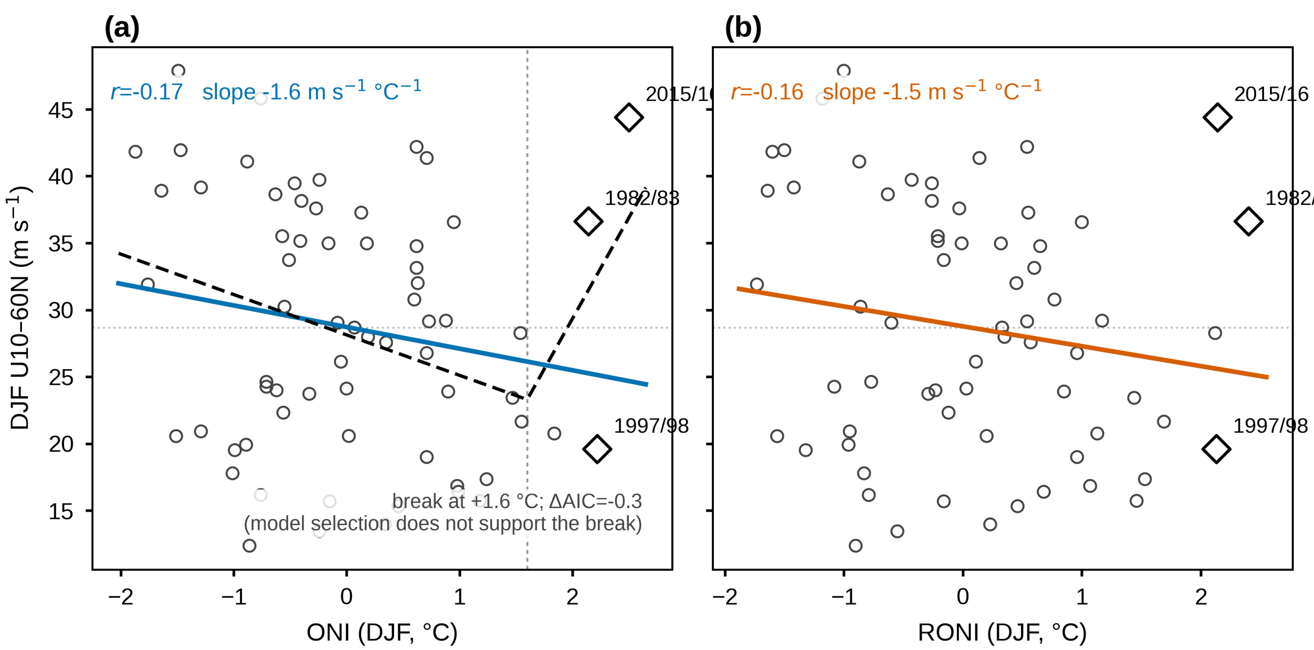

Figure 7. The continuous relationship between ENSO amplitude and polar vortex strength, winters 1959/60–2023/24 (*n*=66). (a) Scatter of ONI(DJF) against DJF U10–60N; the solid line is the linear fit and the dashed line the hinge model that allows a break at +1.6 °C. When the break point is counted as a free parameter, model selection does not support the break (ΔAIC=−0.3). (b) The same relationship using RONI. Diamonds mark the ONI≥+2.0 super winters. No simple relationship in which the vortex weakens systematically as El Niño amplitude increases is apparent, and the three super winters occupy very different vortex strengths (section 5). Data: NOAA CPC (ONI, RONI; ERSSTv6), NCEP/NCAR Reanalysis-1 (U10–60N; NOAA PSL); accessed 28 August 2026. Quantitative figure.

6. SSW Typology: A Subseasonal Descriptor

In an SSW the vortex is either pushed off the pole (displacement; predominantly wave-1) or separated into two cores (split; predominantly wave-2). Whether that morphology matters at the surface is unsettled: reanalysis composites give sharper Eurasian cooling and an earlier downward response for splits (Nakagawa and Yamazaki 2006; Mitchell et al. 2013; Seviour et al. 2013; Hall et al. 2021), whereas a zonal-mean criterion (Charlton and Polvani 2007), large model ensembles (Maycock and Hitchcock 2015; White et al. 2019) and predictive tests (Lehtonen and Karpechko 2016) find no difference of practical use. White et al. (2021) reconcile the two positions on the time axis: splits descend immediately and displacements with a lag of one to two weeks, while beyond three to four weeks the response becomes insensitive to morphology.

Because the classification is itself method-dependent in borderline cases (Charlton and Polvani 2007; Mitchell et al. 2013; Baldwin et al. 2021) and the catalog cannot test the ENSO–type link (Barriopedro and Calvo 2014), SSW type is best treated as a subseasonal descriptor on the 0–2-week scale rather than as a seasonal predictor. This section is therefore ancillary to the main argument: from a Turkish perspective the operative question is not morphology but whether an event couples downward and reverses the NAO. Appendix B (Table B1) summarizes the literature composites and Figure 4 the morphologies.

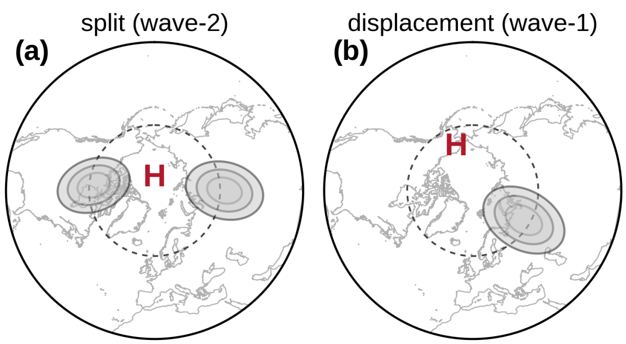

Figure 4. The two morphologies of major SSW events in north polar projection. (a) Split: the vortex separates into two cores, predominantly under wave-2 forcing. (b) Displacement: the vortex is pushed off the pole, predominantly under wave-1 forcing. H marks the center of the height anomaly. The method dependence of the classification and the discussion of the surface signature are given in section 6. This is a conceptual schematic: it is not a composite map produced from numerical fields and cannot be used for quantitative interpretation (section 2.3).

7. European–Turkish Teleconnections: The Anatomy of an Indirect Chain

The most direct quantitative link between the vortex state and Mediterranean precipitation is Zhang et al. (2024): in weak-vortex composites the Atlantic jet shifts southward, and total and extreme precipitation increase over the northern Mediterranean landmass while decreasing north of 45°N, with the moisture budget attributing the dominant contribution to changes in vertical motion. Their model experiment also marks the limit of the chain: WACCM reproduces the stratospherically sourced wave train descending from Greenland to Europe but not the bottom-up tropospheric branch, so the observed dipole cannot be attributed entirely to the stratosphere.

At the Turkish end the chain closes through the NAO/AO: the negative relationship between winter precipitation and the NAO is well documented at the national scale (Türkeş and Erlat 2003), as is the link between the AO and mean winter temperatures (Türkeş and Erlat 2008). The most direct source for regional coefficients is Baltacı et al. (2018), who match 94 stations to five teleconnection patterns over 1965–2014 and report $r \approx -0.5$ for western Anatolian precipitation in the negative AO phase, identifying the deepening Genoa cyclone as the carrier; Sezen and Partal (2019) treat eastward-migrating Cyprus lows and the AO/North Sea–Caspian pattern, and the EA/WR pattern dries the western Mediterranean while watering the eastern basin in its positive phase (Krichak et al. 2002; Trigo et al. 2006). At the event scale, Kömüşcü and Oğuz (2021) document how a vortex disruption combined with an omega block produced extreme cold and snowfall over Türkiye in 2018/19.

Beyond these, no peer-reviewed study directly linking SSW type or QBO phase to Turkish precipitation and temperature at the station scale was identified among the sources searched; this is not evidence of absence, since the search does not rest on a systematic protocol. The regional inference here therefore has two layers: the coefficients measured at the reanalysis scale in section 7.1, and the mechanism chain vortex → downward coupling → NAO/AO → Mediterranean storm track → Genoa/Cyprus cyclogenesis → Turkish surface climate, every link of which can attenuate the signal.

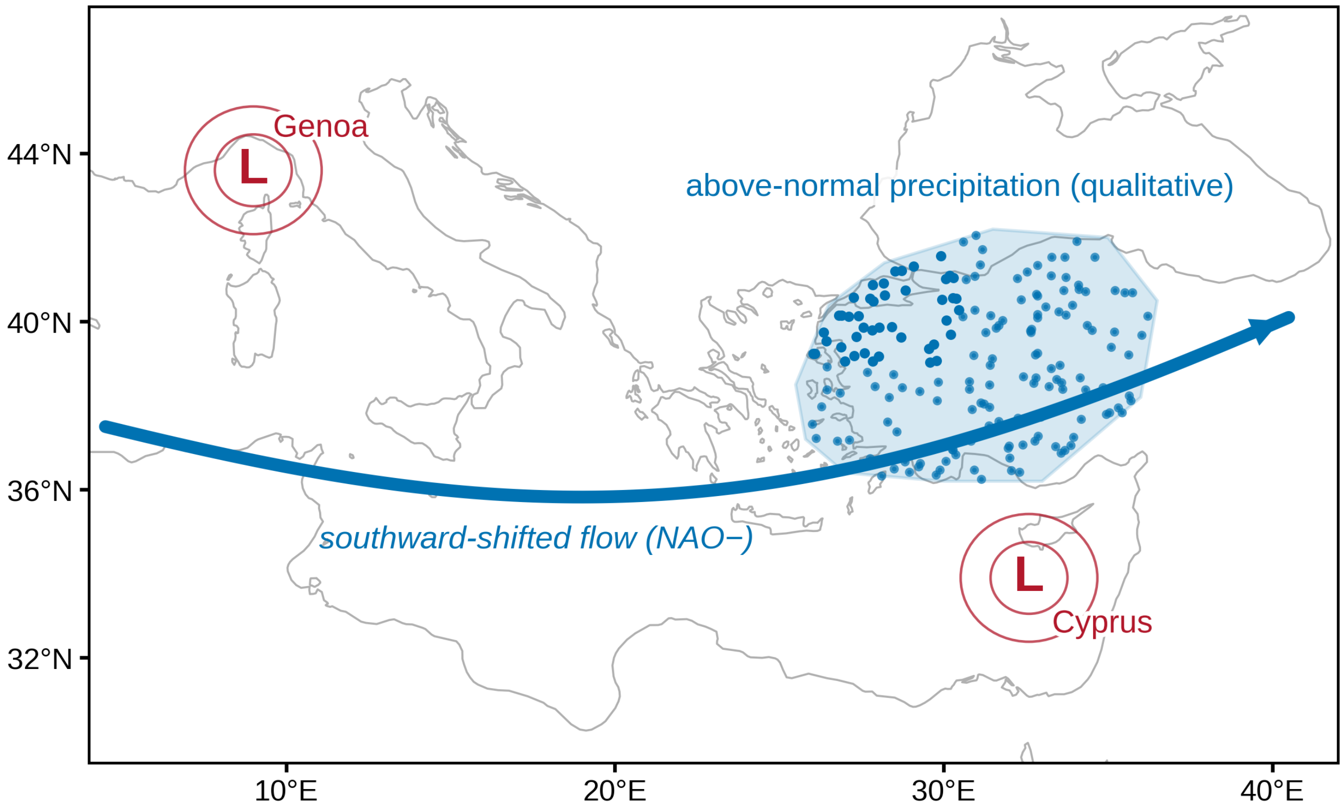

Figure 5. The Mediterranean storm track and the eastern Mediterranean/Türkiye precipitation window under a negative NAO regime. The southward-shifted flow, the Genoa and Cyprus cyclogenesis centers and the above-normal precipitation tendency concentrated around the Marmara–Aegean region are shown qualitatively. The quantitative counterpart of this end of the chain, measured with ERA5, is given in section 7.1 and Figure 9. This is a conceptual schematic: it is not a composite map produced from numerical fields and cannot be used for quantitative interpretation (section 2.3).

7.1 A direct observational test of the vortex–Türkiye link (ERA5)

The terminal link of the indirect chain is measured directly for the first time in this revision: for the winters 1979/80–2021/22 (n=43) the standardized DJF U10–60N was regressed on the monthly ERA5 Z500, precipitation and 2-m temperature fields, with winter-based bootstrap uncertainties and BH-FDR control over the grid (section 2.2). In the circulation layer the result is clear and consistent with the literature: a +1 standard deviation stronger vortex is associated with a positive-NAM-like DJF Z500 pattern — a lowering of up to −28 m around Iceland and a rise of up to +8 m over the Azores ridge and +15 m over central Europe, with a sign close to zero over the eastern Mediterranean (Figure 9a). The coefficient reaches local $p<0.05$ at 42.0% of grid cells and 36.6% pass BH-FDR (α=0.10). JFM preserves the same structure with slightly weaker amplitude (Icelandic center −25 m; local 34.6%, FDR 25.4%), whereas in ND the pattern is weak and mixed (18.8%/16.6%) and should be read with caution because of the partial acausality of the DJF predictor (section 2.2). The concurrent correlation of vortex strength with the NAO follows the same calendar: r=+0.41 in DJF, +0.45 in JFM and +0.10 in ND. In strong-vortex winters the Atlantic–European circulation leans toward the side that relatively suppresses the southerly storm track carrying precipitation into the Mediterranean; the signs reverse symmetrically for a weak vortex.

In the precipitation layer the signal is measurable but modest and spatially heterogeneous: the fraction of FDR-passing grid cells is 1.5% in DJF, 0% in ND and 1% in JFM, and none of the fifteen regional coefficients passes the family-level BH-FDR (α=0.10) threshold (section 2.2); the individual intervals below are to be read as exploratory. In the regional means, DJF gives a consistent dry-signed tendency: a +1 standard deviation stronger vortex means −5.49 mm month^{-1} for the Türkiye box (−6.8% of climatology; 95% CI −10.24/−0.62; p=0.022), −9.69 for the Aegean (−10.0%; −17.26/−1.87) and −5.46 for Marmara (−6.9%; −10.55/−0.39); the intervals for the Mediterranean coast (−8.79; −18.94/+1.69) and the Levant (−2.79; −8.54/+2.98) include zero (Figure 9b, d). In the ND window the signal shifts south: the Mediterranean coast (−11.89; −12.1%; −24.43/−0.56) and the Levant (−6.55; −11.1%; −12.46/−0.50) are off zero while the Türkiye box becomes uncertain (−4.28; −10.89/+2.10). In JFM the intervals of all five regions include zero (Türkiye box −2.25; −6.35/+1.61): the prior expectation that could be derived from the two-pathway literature — a stronger late-winter link — is not confirmed in precipitation, and JFM turns out to be the weakest of the three windows. There is no contradiction between individual intervals that exclude zero and a family-level threshold that is not passed: the signal seen when a single region is examined on its own is not strong enough to clear the multiple-comparison threshold when fifteen regional tests are evaluated together. These coefficients are therefore not a deterministic rule for Turkish precipitation but a probability shift whose sign is consistent and whose statistics are fragile. For weak-vortex winters the sign of every coefficient reverses: −1 standard deviation means a wet-signed tendency of order +5.5 mm month^{-1} for the Türkiye box in DJF. The contribution of sea cells in the boxes has been separated by a land-masked repetition (Table C3): the DJF coefficients are almost unchanged under masking (Türkiye −5.55 [−9.98/−0.95], Aegean −9.10 [−15.84/−2.10], Marmara with four land cells −5.64 [−11.03/−0.16]), whereas the southern-coast signal of the ND window weakens and its interval comes to include zero (Mediterranean coast from −11.89 to −7.49 [−18.17/+2.39]; Levant from −6.55 to −4.24 [−8.97/+0.69]); the "southward shift" in ND is therefore carried partly by sea cells and is more fragile than the midwinter result.

The role of the NAO differs by window. In DJF, controlling for the NAO barely changes the Türkiye coefficient (Model A −5.49 → Model B −5.28) and the bootstrap interval of the indirect component includes zero (−0.17; −2.37/+1.75): the midwinter link appears to carry a component that is not reducible to the monthly NAO index; with n=43 and coefficients that do not pass family-level BH-FDR, that component is an interesting signal to be tested, not an established finding. In JFM the picture is the reverse: adding the NAO erases the Türkiye coefficient (−2.25 → +0.10) and the indirect component is off zero (−2.17; −5.62/−0.04; for Marmara −4.07; −8.59/−0.85) — in late winter the U10 coefficient disappears once the NAO is included. This is an expected result: the relationship of Turkish winter precipitation to the NAO/AO, of order −0.5, is a known channel (Türkeş and Erlat 2003; Baltacı et al. 2018), and the JFM erasure shows that the late-winter link is consistent with variance shared through that channel; it does not prove one-way causal mediation. This is an observational Model A/B decomposition, not a causal path analysis (section 2.2); still, the fact that the "descent through the NAO" expectation of downward coupling is met in late winter and not in midwinter is a distinction worth recording for the mechanism debate. The intuitive reading is that in late winter a substantial part of the vortex–Turkish precipitation relationship appears to carry the same information channel as the NAO-measured component of the Atlantic–European circulation. This pattern is consistent with the interpretation that the connection is an indirect route carried through the NAO; it is not proof of mediation.

The temperature layer is secondary: although 17.9% of grid cells are locally significant in the DJF T2m pattern, only 2.0% pass the FDR criterion, and the Türkiye regional coefficients are indeterminate in all windows (DJF −0.22 K, 95% CI −0.57/+0.10; JFM −0.23; −0.59/+0.16). Taken together, a strong vortex is associated, through a +NAM circulation pattern in which more than a third of the grid cells pass FDR, with a dry-signed probability shift over Türkiye in midwinter of order 7–10% of climatology, and with a symmetric wet-signed shift under a weak vortex; the signal moves to the southern coastal belt in November–December and disappears at the regional scale in January–March. Appendix C gives the full coefficient table and the ND/JFM maps.

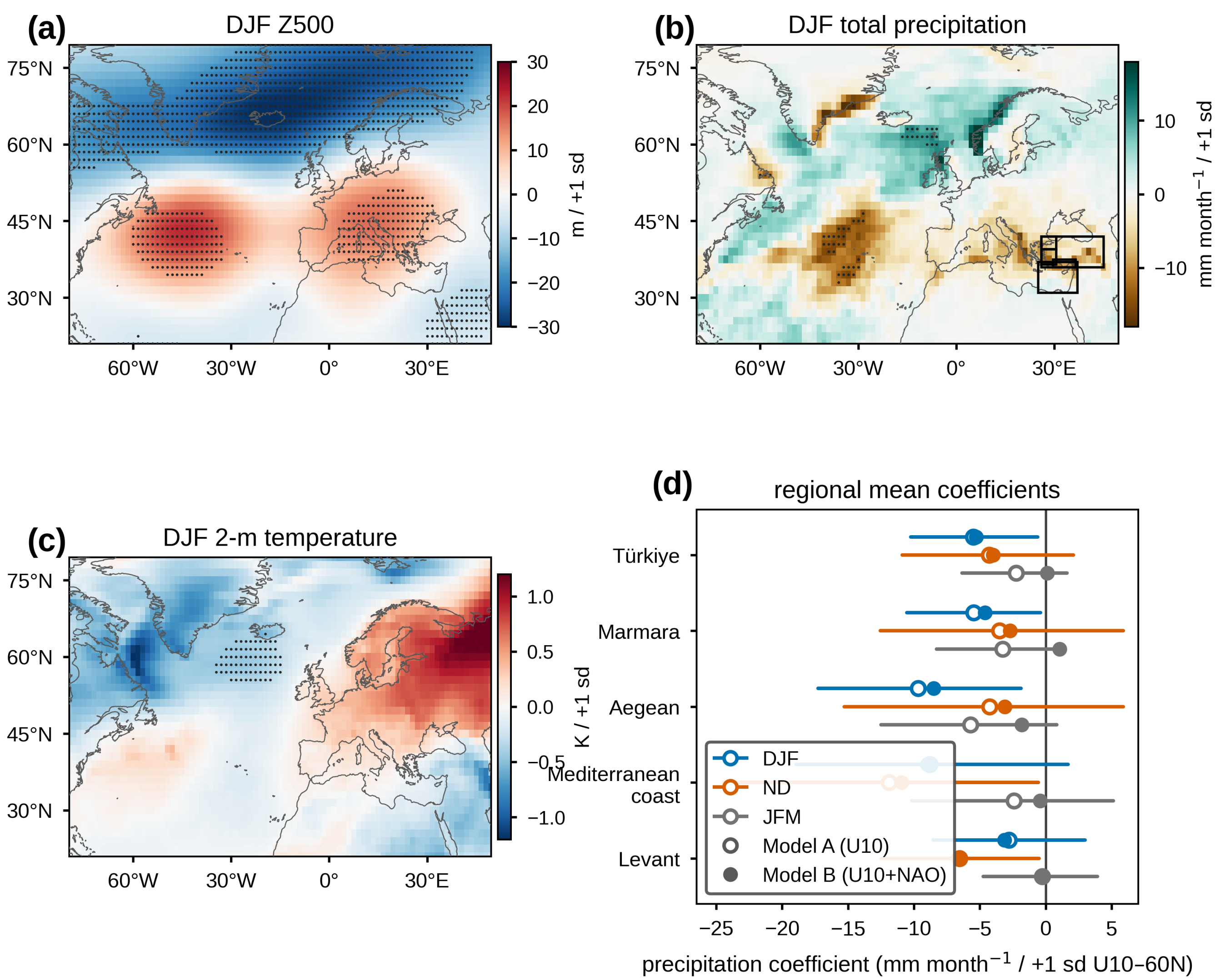

Figure 9. The concurrent regional signature of vortex strength in ERA5: regression on standardized DJF U10–60N, winters 1979/80–2021/22 (n=43; anomalies relative to the 1991–2020 climatology). (a) DJF Z500 coefficient (m per +1 sd); stippling marks grid cells whose winter-based bootstrap 95% interval excludes zero and which pass the BH-FDR (α=0.10) criterion. (b) DJF precipitation coefficient (mm month^{-1} per +1 sd) and the five a priori regional boxes. (c) DJF 2-m temperature coefficient (K per +1 sd). (d) Regional mean precipitation coefficients and their 95% bootstrap intervals; open symbols denote Model A (U10 only) and filled symbols Model B (U10 + NAO); colors denote the DJF/ND/JFM windows. The figure shows the vortex → 500-hPa circulation → Turkish precipitation/temperature links in a single frame; the circulation pattern in (a) passes the BH-FDR criterion at 36.6% of grid cells, whereas the corresponding fraction for the precipitation pattern in (b) is 1.5% — the circulation link is markedly more robust than the precipitation link. The regional boxes are cosine-latitude-weighted full-area means; no land–sea mask is applied. Signs reverse for weak-vortex winters. Data: ERA5 (WeatherBench2 1.5° monthly derivative; Hersbach et al. 2020; Rasp et al. 2024), NCEP/NCAR R1 (U10), CPC (NAO); accessed 29 August 2026. Quantitative figure.

8. Winter 2026/27: A Prospectively Defined Conditional Observational Update

8.1 Initial conditions (August 2026)

As of late August 2026, Niño-3.4 stands at +2.7 °C weekly and +2.03 °C for the July monthly mean; CPC keeps the probability of the "very strong" category above 90% and the October–December RONI median at +2.66 °C (interquartile range +2.37/+2.95), and assigns a 69% probability to a historic peak exceeding all events since 1950; ECMWF members place the Niño-3.4 peak in the +3.5–4.5 °C band; in the IRI plume 25 of 26 models fall in the "very strong" category for October–December and 15 give +3.0 °C or more; and MEI.v2 reaches +2.41 for June–July 2026, the highest June–July value in the post-1979 record. This amplitude offers a strong opportunity to update the conditional expectations of sections 3 and 5, but is not by itself a mechanism-separating experiment. On the QBO side the westerly regime is descending from above — the westerly front was at 40 hPa in July (+9.0 m s^{-1}; 30 hPa +14.3) and the 50-hPa easterly has weakened to −6.5 m s^{-1} — and a simple descent extrapolation predicts that 50 hPa will turn westerly in November–December. The vortex is on its climatological schedule, with no evidence of early formation in mid-August analyses. Table 4 places these initial conditions alongside the historical analogs.

Table 4. Super El Niño winters and 2026/27. ONI: NOAA CPC, ERSSTv6, `oni.ascii.txt`, accessed 28 Aug 2026. QBO50(Nov): sign of the CPC/CDAS 50-hPa November mean. The NAO column runs November–December → January–March.

Winter	**ONI (DJF)**	QBO50 (Nov)	Major SSW	NAO (ND→JFM)	Note
1982/83	+2.1	W	None	+1.69 → +0.67	The RONI record (+2.40) belongs to this event
1997/98	+2.2	W	None	−0.93 → +0.38	Exception to the composite: entered the winter with a negative NAO
2015/16	+2.5	W	None	+1.99 → +0.81	February 2016 QBO disruption; record-strength vortex
2023/24	+1.8	E	16 Jan [D]; 4 Mar [S]	+0.81 → +0.36	Sub-super analog; two events under easterly QBO
2026/27	to be monitored (forecast ≥ +2.0)	W (descending; to be monitored)	to be monitored	to be monitored	RONI OND median +2.66; QBO disruption is the wild card

8.2 Competing explanations

Four explanations are on the table for the SSW-free super winters of the record, and 2026/27 cannot deliver a single-winter verdict among them. If the expected wQBO materializes, H1 and H2 generate expectations in the same direction — less favorable conditions for an SSW and a relatively stronger vortex — so the winter will not separate them; the more discriminating natural case would be a genuine super El Niño under eQBO. The function of 2026/27 is narrower: to show to what extent conditional expectations defined before the outcome was known gain or lose support. The framework below is a sequential observational evidence update, not a confirmation/falsification scheme.

H1 — Saturation/nonlinearity. As ENSO amplitude increases, the effective planetary-wave forcing transmitted to the stratosphere may not grow proportionally, one candidate mechanism being a loss of efficiency in the constructive interference of the ENSO-driven wave pattern with climatological wave-1 (Zhou et al. 2019). This study does not measure that mechanism: the ONI/RONI–U10–60N relationship and the segmented fit test only the downstream vortex-level signature, and $r=-0.17$ with $\Delta AIC=-0.3$ provide no support for it. If U10–60N in 2026/27 remains close to the historical super-winter range despite record amplitude, that is compatible with H1 without being mechanistic evidence, whereas a markedly weak vortex or a major SSW would reduce the weight given to a simple plateau expectation. A more direct test requires eddy heat flux ($v'T'$) at 100 hPa in the 45–75°N band together with the EP flux and the wave-1 interference term.

H2 — QBO modulation. The Holton–Tan framework requires the QBO to be seen not as a deterministic switch but as a background condition that probabilistically alters the sensitivity of the polar vortex to planetary-wave forcing. In our own data, under the main November 50-hPa definition the eQBO/wQBO SSW risk is 12/19 against 13/26 (RR=1.26; 95% CI 0.75–2.12); in the 30-hPa long record RR=1.48 (0.94–2.32). Although the direction is largely consistent, the intervals include 1 and the ENSO×QBO interaction cannot be resolved. A major SSW under wQBO in 2026/27 therefore does not falsify H2; it merely breaks the present n=3 "super El Niño + wQBO + no SSW" pattern and reduces the relative weight given to the QBO explanation. Conversely, the absence of an SSW under wQBO neither confirms H2 nor separates H1 from H2. If the phase remains easterly or the pre-winter profile turns easterly, the case becomes more discriminating for H2; even then a single winter is not a verdict on a probabilistic hypothesis but a small information update quantified in Appendix D. The way to resolve this question at the scale the observational record cannot reach is large-ensemble hindcasts: the ECMWF SEAS5 retrospective forecast set for 1981–2016 with 51 members (Johnson et al. 2019) supplies of order 1,800 model winters and, because it carries the ENSO and QBO initial conditions, fills the ENSO×QBO cells with hundreds rather than tens of winters; the C3S multi-system set multiplies this (see section 9).

H3 — Ordinary/internal variability. Blocking sequences and the internal timing of wave packets may dominate SSW occurrence, so the clustering across three super winters may need no special mechanism; the base rate of 0.58 alone makes a 3/3 SSW-free run a one-in-fourteen outcome. The permutation reference of 0.06–0.09 for the 3/3 wQBO match points the same way, and the counterexamples of 1957/58 (wQBO with an SSW) and 1991/92 (eQBO without an SSW) keep H3 on the table. Of the four explanations this is the one the present evidence is least able to exclude.

H4 — El Niño flavor. The fourth candidate is independent of the QBO: observational and model studies report that Central-Pacific-weighted El Niños do not weaken the stratospheric vortex as Eastern Pacific events do, and may even strengthen it (Hegyi et al. 2014; Garfinkel et al. 2013; Iza and Calvo 2015). Among the three super winters, the mixed Central/Eastern Pacific structure of 2015/16 (Paek et al. 2017) makes this explanation particularly apt for that event; 1982/83 and 1997/98 are classical Eastern Pacific events. For 2026/27 H4 requires monitoring, beside the Niño-3.4 amplitude, the Niño-3/Niño-4 separation and the longitude of the convective center; because it is independent of QBO phase it is not pushed in the same direction as H2, and it is the only candidate explanation capable of distinguishing the “true exception” status of 2015/16 from the QBO disruption.

8.3 Prospectively defined discriminating observations and evidence updating

The following outcomes will be interpreted with the same criteria before the winter takes place; the operational definitions of those criteria (which level, which month, which SSW definition, which ruler, which likelihood ratios) are fixed in Appendix D as a prospectively defined protocol, and only that protocol will be applied at the end of the winter. (i) If the November 50-hPa mean remains easterly, or a persistent easterly layer appears in the 40–50-hPa descent profile, 2026/27 becomes more discriminating with respect to H2; the cleanest natural separation remains a genuine super El Niño under eQBO. (ii) If wQBO materializes and a major midwinter SSW occurs, H2 is not thereby falsified; the present 3/3 pattern breaks, the weight given to QBO conditioning decreases, and the simple saturation expectation also weakens. (iii) The absence of an SSW under wQBO together with a strong U10–60N would extend the pattern by one event and place additional pressure on H3, but would not separate H1 from H2. (iv) If U10–60N remains close to the historical super-winter distribution despite record ENSO amplitude, that will be counted as compatible with the vortex-level expectation of the simple saturation scenario, whereas a marked weakening will be counted as less compatible. Because planetary-wave forcing is not measured directly, this comparison will not be converted into a mechanistic verdict on H1. The differences between the RONI and ONI rulers, the counterexamples of 1991/92 and 2023/24, and the Niño-3/Niño-4 structure of the 2026/27 event (H4) will be retained as the sensitivity limits of the interpretation. Given the power calculation of section 4, a single winter will move the relative weight on H1–H4 by a few percent at most; the value of the exercise lies in the registration and in the discipline it imposes on the post-winter reading, not in the verdict.

From an eastern Mediterranean perspective the inference is now quantified but still cautious. Section 7.1 produces direct reanalysis-scale coefficients between U10–60N and Türkiye box-mean precipitation: in DJF a +1 standard deviation stronger vortex means −5.5 mm month^{-1} for the Türkiye box, and a weak vortex a symmetric wet-signed tendency — of order 7% of climatology, probabilistic rather than deterministic. A station-scale coefficient has still not been produced, and every link of the chain can dilute the signal. The 2026/27 monitoring set should therefore follow, more closely than El Niño amplitude itself, the late-November QBO profile, jumps in wave-driven heat transport at 100 hPa in the 45–75°N band, the 10-hPa 60°N wind, the downward NAM/AO signal and the intraseasonal direction of the NAO and Mediterranean circulation. The early-winter r=+0.21 and late-winter r=−0.12 values are not a deterministic precipitation calendar for Türkiye; they show only why intraseasonal differentiation must be taken into account in regional interpretation. Two qualifications belong in that monitoring set from the outset. The North Atlantic storm-track response to an SSW is itself modulated by the state of the Pacific (Afargan-Gerstman and Domeisen 2020), so events falling in El Niño winters need not project on the eastern Mediterranean as events in neutral winters do, and the surface variance attributable to SSWs has to be separated from that attributable to ENSO itself (Polvani et al. 2017). The regional carrier is also not the NAO alone: the North Sea–Caspian pattern (Kutiel and Benaroch 2002) and Cyprus lows mediate much of the Anatolian response, and a lagged 0–60-day composite of Turkish station precipitation on major events over 1958–2026 is the natural next test.

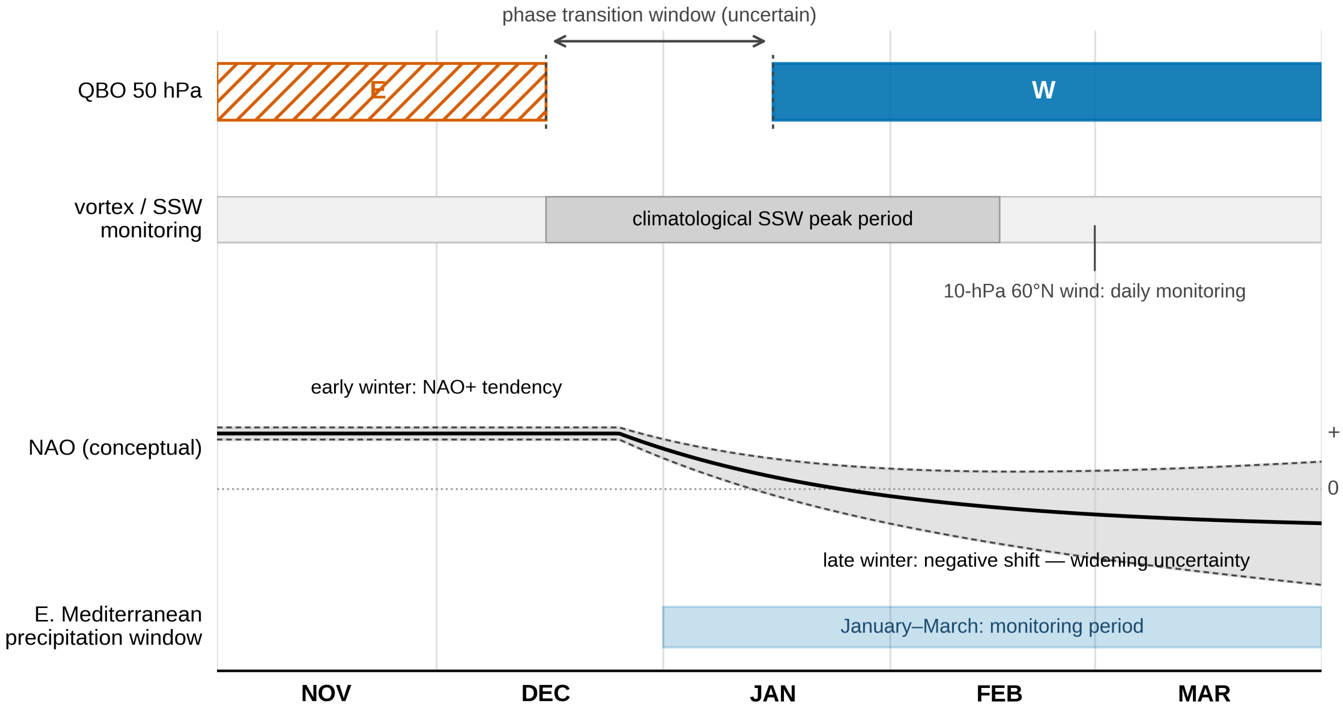

Figure 6. Monitoring calendar for the winter of 2026/27. The rows show, in order, the expected evolution of the 50-hPa QBO phase and the uncertainty of the phase transition window; the vortex/SSW monitoring period together with the climatological peak range of SSWs; the conceptual evolution of the NAO with a widening uncertainty fan; and the eastern Mediterranean precipitation window. The calendar is not a forecast but the order in which the discriminating observations defined in section 8.3 will be monitored. This is a conceptual schematic: it is not a composite map produced from numerical fields and cannot be used for quantitative interpretation (section 2.3).

9. Discussion

The ENSO–NAO result is not a discovery but an independent and repeatable reproduction (Moron and Gouirand 2003; Ayarzagüena et al. 2018; King et al. 2018; Mezzina et al. 2020), and it should be read through the difference between the two intraseasonal windows rather than through the strength of the individual correlations. In early winter r=+0.21 and in late winter r=−0.12, and both individual confidence intervals include zero; the paired difference, by contrast, is Δr=+0.33 (95% CI +0.08/+0.56) and stays off zero under a moving-block bootstrap. This does not show that ENSO deterministically causes a positive NAO in early winter and a negative NAO in late winter. The more defensible conclusion is that the ENSO–NAO relationship can differentiate systematically within the same winters and that the DJF mean (r=−0.04) can mask that structure by adding opposing tendencies together. That the late-winter behavior in the composites is more often a weakening than a full sign reversal, and that exceptions such as 2015/16 exist, preserves that limit.

For the QBO the seasonal-mean surface correlation is close to zero (QBO50×AO r=−0.01), whereas the winter-based probability of a major SSW appears higher under eQBO. Under the main November 50-hPa definition RR=1.26 (95% CI 0.75–2.12) and in the 30-hPa long record RR=1.48 (0.94–2.32); the value of 1.71 under the DJF definition, which overlaps the outcome period, is an upper bound. That the confidence intervals include 1 shows that the magnitude of the effect cannot be pinned down with the present record. The QBO is therefore not a “switch” but a conditioner whose direction is largely consistent across the main definitions and whose probability shift is of uncertain magnitude. The ENSO×QBO interaction cannot be resolved because of both the small cells and the definition sensitivity; the present data neither prove nor exclude an interaction. The power calculation fixes this quantitatively: a difference of the order of a risk ratio of 1.26 requires about 450 independent winters, and a single winter moves the likelihood ratio by only about 1.2. For that reason 2026/27 is not a “test” and the paper does not present it as one; the scale at which the question can be resolved is that of large-ensemble hindcasts. ECMWF SEAS5 alone (1981–2016, 51 members; Johnson et al. 2019) supplies about 1,800 model winters and, because it carries the ENSO and QBO initial conditions together, fills the ENSO×QBO cells with hundreds of winters; the C3S multi-system set multiplies this. Richter et al. (2011) and Kumar et al. (2022) opened the model side of this route; the core of the follow-up study lies on this line.

The two components of the super El Niño pattern do not carry the same epistemic weight, and neither rises to the level of a paradox: the SSW-free component has a chance probability of $0.42^3 \approx 0.07$ against the 58% base rate, and the three winters are heterogeneous in vortex strength (1997/98 conforms to the canonical chain, 1982/83 is intermediate, 2015/16 is the true exception). That 1982/83, 1997/98 and 2015/16 are 3/3 wQBO and 3/3 SSW-free under ONI≥+2.0 is notable, but n=3 keeps it at the level of a hypothesis-generating pattern. The QBO-phase result is preserved under the 50-hPa November, November–December and DJF and the 30-hPa November definitions, while under 30-hPa DJF 1997/98 changes phase; the phrase "robust across all QBO definitions" should therefore not be used. The sequence-preserving permutation reference of 0.06–0.09 does not exclude chance. More importantly, the RONI≥+2.0 ruler raises SSW-freeness to 4/4 by adding 1991/92 while reducing wQBO purity to 3/4. The "super El Niño–no SSW" pattern thus strengthens under a change of index while the hypothesis that "this is explained by wQBO" weakens. Under the expected wQBO, 2026/27 will not cleanly separate these two explanations; the more discriminating future case is an eQBO super El Niño. The mixed Central/Eastern Pacific structure of 2015/16 required a fourth explanation independent of the QBO (H4) in order to separate its exception status from the QBO disruption, and that explanation has been added to section 8.2.

In the saturation debate, U10–60N measures only the downstream vortex response. The ONI–U10 relationship is r=−0.17 (p=0.16) and the segmented fit gives ΔAIC=−0.3; the vortex-level continuous signature of a simple "weakens with amplitude, then plateaus" scenario is therefore not supported in the present observational record. This result is not a direct rejection of the planetary-wave forcing mechanism. A more direct test of H1 should examine wave-driven meridional heat transport at 100 hPa in the 45–75°N band (v′T′), the EP flux and planetary wave-1 amplitude and, where possible, the constructive interference of the ENSO-induced anomaly with the climatological wave-1 across amplitude. In the continuous regression adding wQBO raises R^2 from 0.002 to 0.126 with a coefficient of +6.79 m s^{-1} (95% CI +1.19/+12.39); this measurable relationship is interesting, but it is produced from NCEP/NCAR Reanalysis-1 alone. The coefficient magnitude, the super-winter percentiles and the ONI/RONI–U10 results should not be described as "reanalysis-independent" or "robust across reanalyses" until they have been re-tested on ERA5 and, where possible, JRA-55; the ERA5 record extending back to 1940 (Soci et al. 2024) and JRA-3Q (Kosaka et al. 2024) are better suited to this quantity, and re-derivation of the U10–60N series from ERA5 is recorded in Appendix D as a pre-submission step. A first step has been taken at the predictor level in this revision: the NCEP R1 U10 series was re-derived independently and matched the catalog exactly, and the R1–R2 comparison gives r=0.9997, a mean difference of +0.15 m s^{-1} and an RMS of 0.28 m s^{-1}; the derivation of the 10-hPa field from ERA5 is a predefined future step.

The limitations combine at the level of sample, data product and regional inference. The ENSO×QBO cells are small; the SSW catalog does not extend before 1958 nor the 50-hPa QBO series before 1979; the split/displacement classification is method-dependent, and its surface effect, especially at the seasonal scale, is not fully settled across model and reanalysis studies. At the regional end this revision has taken a step: the core of the design proposed as future analysis in the second round — matching the vortex metric with ERA5 fields in a multivariate framework that considers the NAO/AO jointly — has been implemented in section 7.1 and has for the first time turned the link between vortex strength and Türkiye box-mean precipitation into coefficients with confidence intervals. What has not been implemented is recorded with the same clarity: the analysis is at the reanalysis grid scale, not the station scale; it is built on concurrent seasonal windows, and the 0–60-day lagged/distributed-lag design and event-based composites remain in the future; the NAO "mediation" is an observational Model A/B comparison, not a causal path analysis; the ND window is partly acausal when built on the DJF predictor (the pattern correlation with a concurrent predictor drops to 0.68); at 1.5° the regional boxes are coarse; the mean in all five boxes is a cosine-latitude-weighted full-area mean that includes sea cells; the land-masked repetition (Table C3) preserves the DJF coefficients while showing that part of the ND southern-coast signal comes from sea cells, and the Marmara box under the mask consists of four cells; coastal representation is limited at this resolution, and a repetition on MGM long station series and E-OBS is future work. In the family of fifteen regional coefficients none passes BH-FDR (α=0.10); individual intervals that exclude zero are exploratory. Section 7.1's own finding also disciplines the interpretation: the prior expectation of a "stronger late-winter link" was not confirmed in precipitation, and JFM turned out to be the weakest of the three windows; by contrast, controlling for the NAO erases the coefficient only in JFM — the distinction between a midwinter link that carries a component not reducible to the monthly NAO index and a late-winter coefficient erased once the NAO is included coincides in late winter with the "descent through the NAO" expectation of the downward-coupling literature and is left as an observation capable of separating mechanism hypotheses; the midwinter non-NAO component should be kept at the level of "interesting, to be tested". The regional backbone of the follow-up study is a 0–60-day lagged composite analysis of SSW and weak-vortex events over Turkish stations (1958–2026, ERA5 and MGM); Afargan-Gerstman and Domeisen (2020), who show that the Atlantic response to SSWs in El Niño winters differs from that of other SSWs, and Polvani et al. (2017), who separate SSW from ENSO effects, indicate the first place to look for that distinction in the eastern Mediterranean; the NAM from 100 hPa to the surface as the downward-coupling indicator, Cyprus lows and the North Sea–Caspian pattern (Kutiel and Benaroch 2002; Sezen and Partal 2019) as the regional carriers, and the ECMWF extended-range and S2S databases for real-time monitoring are parts of this design.

10. Conclusions

The findings can be summarized under five headings; under each, the observational result is separated from the stronger claim that cannot be drawn from it.

1) Intraseasonal ENSO–NAO structure. The ONI–NAO correlation is r=+0.21 in early winter and r=−0.12 in late winter; both individual relationships are weak and their confidence intervals include zero. By contrast the paired difference over the same winters is Δr=+0.33 (95% CI +0.08/+0.56) and is preserved under a moving-block bootstrap. What is strong is therefore not the individual correlations but the differentiation between early and late winter; this structure is an independent reproduction of the published literature (Moron and Gouirand 2003; Ayarzagüena et al. 2018), and our contribution is the interval on the paired difference. The finding does not show that ENSO causes a particular NAO sign; it shows that a single DJF mean (r=−0.04) can conceal opposing intraseasonal tendencies. Its physical counterpart is consistent with the tropospheric pathway coming to the fore in early winter and the pathway descending through the stratosphere in late winter; its limit is that the individual relationships remain weak.

2) QBO / Holton–Tan. The QBO50×AO seasonal-mean correlation is approximately zero (r≈−0.01). In winter-based major-SSW risk the main November 50-hPa definition gives RR=1.26 (95% CI 0.75–2.12) and the 30-hPa long record RR=1.48 (0.94–2.32); RR=1.71 under the DJF definition, which overlaps the outcome period, should be read as an upper bound. Because the intervals include 1 the effect size is not certain, and detecting a difference of this size requires about 450 independent winters; the observational record cannot settle the question on its own, and a single winter moves the likelihood ratio by only ~1.2. Westerly QBO does not prevent a sudden stratospheric warming; in the present record it only shifts the probability weight. The QBO is here not a forcing that shifts surface indices deterministically but a conditioner that can alter event probabilities by a limited and uncertain amount; the ENSO×QBO interaction cannot be resolved with the present data. Therefore a single SSW under wQBO in 2026/27 will not falsify H2, and the absence of an SSW will not confirm it.

3) The super El Niño pattern. That 1982/83, 1997/98 and 2015/16 are 3/3 wQBO and 3/3 SSW-free under ONI≥+2.0 in the main definition is not a paradox: SSW-freeness has a chance probability of $0.42^3 \approx 0.07$ against the 58% base rate, the three winters are heterogeneous in vortex strength and the only true exception is 2015/16, the winter in which the QBO was disrupted; because n=3 the pattern is a hypothesis-generating observation rather than evidence, and for 2015/16 the El Niño flavor (H4) is a candidate explanation independent of the QBO. Under RONI≥+2.0, 1991/92 enters the set: SSW-freeness strengthens to 4/4 while wQBO purity falls to 3/4. The SSW-free component thus strengthens under a change of ruler while QBO-phase purity weakens; the two propositions are not equally index-robust. The 3/3 wQBO pattern is preserved under the 50-hPa November, November–December and DJF and the 30-hPa November definitions, but under 30-hPa DJF 1997/98 changes phase. The sequence-preserving 0.06–0.09 permutation reference does not exclude chance. The more discriminating future observation is a true super El Niño under eQBO conditions.

4) Saturation and the continuous vortex. The ONI–U10–60N relationship is weak and consistent with zero (r=−0.17; p=0.16); the segmented model does not outperform the linear one (ΔAIC=−0.3). The U10 values of the super trio are not homogeneous. The expected continuous vortex-level signature of a simple saturation scenario is therefore not supported in the observational record; but the analysis is not a direct test of planetary-wave forcing: U10–60N measures not the forcing the waves apply to the vortex but the vortex's final response to it. In the joint sample the ONI-only model gives R^2=0.002 while adding wQBO raises R^2 to 0.126 with a wQBO coefficient of +6.79 m s^{-1} (95% CI +1.19/+12.39; p=0.019); the additional explanatory power of the ENSO×QBO term is very small. Because this regression rests on NCEP/NCAR Reanalysis-1, the coefficient and the super-winter percentiles should be re-tested on ERA5 and, where possible, JRA-55; product-independent robustness has not yet been demonstrated.

5) 2026/27 and the eastern Mediterranean. No direct "El Niño amplitude → precipitation/temperature" rule can be drawn for Türkiye; the vortex-strength → Turkish-precipitation link, by contrast, has been tested directly in this revision and a quantitative bridge for the stratosphere–Türkiye chain has been built for the first time — a bridge built with a single reanalysis product, over a single period and without station verification. In DJF, +1 standard deviation of vortex strength is associated with a positive-NAM Z500 pattern in which 36.6% of grid cells in the Atlantic–European sector pass the BH-FDR (α=0.10) threshold and with a precipitation anomaly of −5.5 mm $month^{-1}$ [95% CI −10.2/−0.6] in the Türkiye box (Aegean −9.7, Marmara −5.5; in November–December the signal shifts to the Mediterranean coast −11.9 and the Levant −6.6); in weak-vortex winters the signs reverse. The effect sizes are in the band of ~7–12% of the regional climatologies, the DJF coefficients are preserved in the land-masked repetition while the ND southern-coast signal comes partly from sea cells, the fraction of FDR-passing grid cells in precipitation is low, none of the fifteen regional coefficients passes the family-level BH-FDR threshold and the regional signals vanish in January–March: this link is a probabilistic tendency, not a deterministic rule. The strength of evidence is not equal across layers: the 500-hPa circulation link passes the multiple-comparison threshold in more than a third of grid cells, whereas the Turkish precipitation signal is consistent in sign but statistically fragile. The physical chain to be monitored is QBO → planetary-wave forcing → polar vortex → downward stratosphere–troposphere coupling → NAO/AO → Mediterranean storm track → Türkiye; section 7.1 has given a measured magnitude to the terminal link of that chain. 2026/27 is a prospectively defined conditional observational update; a single winter will not pass judgment on any hypothesis but will only update the relative observational weight given to them: wQBO+SSW breaks the present 3/3 pattern and may reduce the relative weight given to H2 but does not falsify it; wQBO+no SSW may extend the pattern but does not separate H1 from H2. The next quantitative step toward reducing regional uncertainty is to test these coefficients at station scale with Türkiye's long station series and a 0–60-day lagged design.

This study shows that ENSO amplitude alone is insufficient to explain the state of the polar vortex, and that the QBO appears in the present record as a more visible but limited and probabilistic conditioner than ENSO amplitude. The super El Niño–no SSW observation is not a paradox but a heterogeneous record, and because of the small sample it has the status of a hypothesis; moreover the SSW-free component is more resistant to the ONI/RONI change of ruler than QBO-phase purity. The present saturation analysis is not a direct mechanistic test of planetary-wave forcing, and the continuous vortex result rests on a single reanalysis product; by contrast the European–Mediterranean end of the chain has been measured independently with ERA5 and the regional effect sizes have been given with confidence intervals (section 7.1). 2026/27 is therefore not a definitive confirmation or falsification experiment but an observational trial in which prospectively defined conditional expectations will be updated against a new extreme observation. The paper's first finding is the verification of a published result; its most original contribution is that the decision rules are fixed in Appendix D before the outcome is known. Its scientific value lies not in extracting a "winning hypothesis" from a single winter but in showing explicitly and reproducibly how the relative observational support given to saturation, QBO modulation and internal variability should be re-weighted as new information arrives.

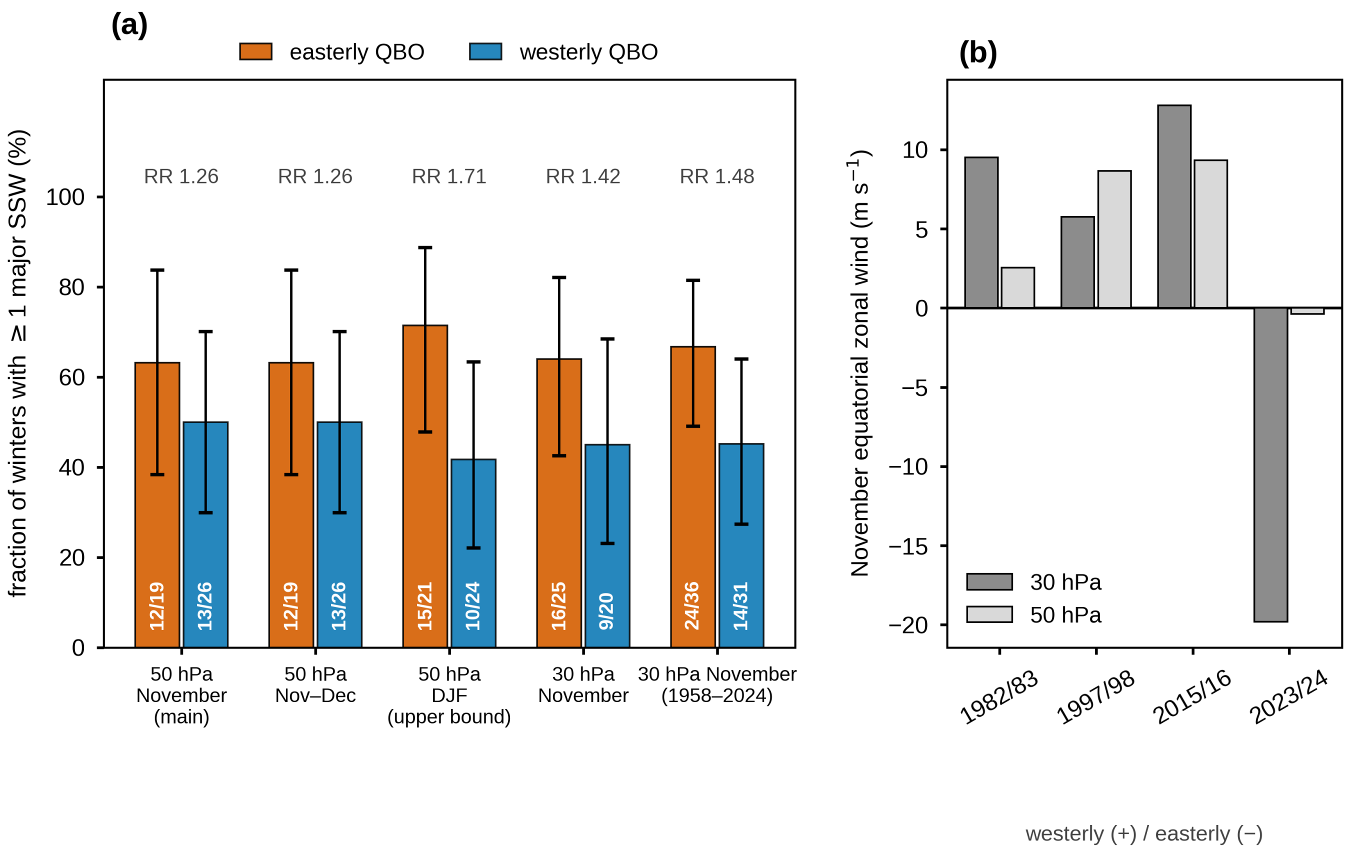

Figure 8. Under all five phase definitions the easterly-QBO side indicates a higher fraction: the direction is relatively consistent, the magnitude uncertain. (a) Sensitivity of the fraction of winters with at least one major SSW to the QBO phase definition; bars are Clopper–Pearson exact 95% intervals and the labels give the numerator and denominator counts. (b) The 30- and 50-hPa November equatorial zonal wind for the super winters and for 2023/24. Panel (b) shows the November classification only; under the 30-hPa DJF sensitivity definition 1997/98 moves to the easterly phase (Table A3), so phase robustness should not be generalized as holding under all definitions. Data: CPC/CDAS (50 hPa, 1979–), NOAA PSL (30 hPa, 1948–), NOAA CSL SSW Compendium; accessed 28 August 2026. Quantitative figure.

Tables

Table 1. Catalog of El Niño winters (ONI_DJF ≥ +0.5; 1951–2024). QBO50(Nov) and QBO30(Nov): sign of the November mean of the 50-hPa (CPC/CDAS, 1979–) and 30-hPa (NOAA PSL, 1948–) equatorial zonal-mean wind; the labels are derived independently of the SSW catalog. U10–60N: 10-hPa 60°N DJF zonal-mean wind, m s⁻¹ (NCEP/NCAR R1; 1959–2024 climatology 28.7 ± 9.3 m s⁻¹). ONI: NOAA CPC, ERSSTv6. All series accessed 28 August 2026.

Winter	**ONI (DJF)**	QBO50 (Nov)	QBO30 (Nov)	U10–60N	SSW (ERA5 central date) [type†]	NAO (ND)	NAO (JFM)	**AO (DJF)**
1951/52	+0.5	—	E	+25.7	—	+0.47	−0.46	+0.20
1957/58	+1.7	—	W	+24.9	8 Feb 1958	+0.42	−1.19	−0.95
1958/59	+0.6	—	E	+30.8	Nov 1958 (absent in ERA5)	+0.47	−0.11	−0.39
1963/64	+0.9	—	W	+36.6	—	−1.59	−1.19	−0.46
1965/66	+1.2	—	E	+17.3	16 Dec 1965; 22 Feb 1966	−0.14	−0.86	−1.50
1968/69	+1.0	—	E	+16.8	28 Nov 1968; 13 Mar 1969	−1.17	−1.31	−2.29
1972/73	+1.6	—	E	+21.6	31 Jan 1973	+0.36	+0.40	+1.09
1976/77	+0.7	—	E	+19.0	9 Jan 1977	−0.72	−0.78	−2.62
1977/78	+0.7	—	E‡	+26.8	—	−0.54	−0.28	−1.20
1979/80	+0.6	E	E	+34.8	29 Feb 1980	+0.77	−0.34	−0.57
1982/83	+2.1	W	W	+36.6	—	+1.69	+0.67	+0.17
1986/87	+1.2	W*	E	+15.7	23 Jan 1987	+1.64	−0.58	−0.85
1987/88	+0.6	W	W	+32.0	8 Dec 1987; 14 Mar 1988	+0.25	+0.54	−0.45
1991/92	+1.5	E	E	+28.3	—	+0.47	+0.60	+1.09
1994/95	+0.9	E	E	+29.2	—	+1.33	+1.11	+0.72
1997/98	+2.2	W	W	+19.6	—	−0.93	+0.38	−0.78
2002/03	+0.9	W	W	+23.9	18 Jan 2003	−0.56	+0.37	−0.65
2004/05	+0.6	W	W	+42.2	—	+0.97	−0.12	+0.11
2006/07	+0.6	W	W	+33.1	24 Feb 2007	+0.89	+0.40	+1.00
2009/10	+1.5	W*	E	+23.4	9 Feb 2010 [S]; 24 Mar 2010 [D]	−0.97	−1.32	−3.42
2014/15	+0.7	E	E	+29.1	—	+1.27	+1.52	+0.85
2015/16	+2.5	W	W	+44.4	—	+1.99	+0.81	−0.01
2018/19	+1.0	E*	W	+16.4	1 Jan 2019 [S]	+0.25	+0.70	+0.18
2019/20	+0.7	W	W	+41.4	—	+0.74	+1.20	+2.08
2023/24	+1.8	E	E	+20.8	16 Jan 2024 [D]; 4 Mar 2024 [S]	+0.81	+0.36	+0.07

ND = November–December; JFM = January–February–March. "—" = no CPC 50-hPa data before 1979; the phase for these winters is derived from 30 hPa only. ‡ = November value very close to zero (−0.3 m s⁻¹), so the classification is borderline. * = the November labels of the two levels disagree; across the full catalog the winters that disagree are 1983/84, 1986/87, 1988/89, 1992/93, 1993/94, 1995/96, 2009/10, 2011/12, 2017/18 and 2018/19. † The split (S) / displacement (D) classification is method-dependent (the zonal-mean criterion of Charlton and Polvani 2007 and the 2-D moment diagnostic of Mitchell et al. 2013 can diverge in borderline cases; see Baldwin et al. 2021); a type is assigned only to recent events for which there is broad agreement in the literature, and disputed cases are marked with an asterisk. The 2023/24 events postdate the compendium (Lee 2025).

Table 2a. Correlations computed in this study. p values are descriptive (section 2.2). Data: NOAA CPC (ONI, NAO, AO, QBO50), NOAA PSL (QBO30); accessed 28 August 2026.

#	Pair	Period	***n***	***r***	***p***	Note
1	ONI(DJF) × NAO(DJF)	1951–2026	76	−0.04	0.74	The seasonal mean masks the relationship
2	ONI(DJF) × NAO(Nov–Dec)	1951–2026	76	+0.21	0.06	Early winter: positive tendency
3	ONI(DJF) × NAO(Jan–Mar)	1951–2026	76	−0.12	0.32	Late winter: reversal toward negative
4	ONI(DJF) × AO(DJF)	1951–2026	76	−0.12	0.30	
5	ONI(DJF) × AO(Jan–Mar)	1951–2026	76	−0.17	0.14	Strengthens in late winter
6	QBO50(ND) × AO(DJF)	1980–2026	47	−0.01	0.94	No surface imprint of Holton–Tan in the seasonal mean
7	QBO50(ND) × NAO(DJF)	1980–2026	47	+0.11	0.46	
8	QBO30(ND) × AO(DJF)	1951–2026	76	+0.06	0.59	Sign in the Holton–Tan direction but negligible
9	ONI(DJF) × U10–60N	1959–2024	66	−0.17	0.16	Vortex-level signature of the simple saturation scenario (Figure 7)
10	RONI(DJF) × U10–60N	1959–2024	66	−0.16	0.19	

Table 2b. Published coefficients (for comparison).

Source	Quantity	Value
Watson and Gray (2014, JAS)	QBO(50 hPa, Nov–Feb) × U(10 hPa, 60°N)	r = 0.58
Scaife et al. (2014, GRL)	GloSea5 ensemble mean × observed DJF NAO	r = 0.62
Butler and Polvani (2011, GRL)	SSW frequency, ENSO / neutral	~2×
Palmeiro et al. (2023, JGR)	SSW per decade: neutral 9.2, EN 8.3, LN 8.2 (1950–2021)	difference not significant
Baltacı et al. (2018, TAC)	AO × western Anatolian winter precipitation	$r \approx -0.5$
Baltacı et al. (2018, TAC)	AO × Black Sea / Aegean warm days	$r = -0.6 / -0.7$
Türkeş and Erlat (2008, TAC)	AO × Türkiye mean winter temperature	negative, regionally variable
Mitchell et al. (2013, J. Climate)	Eurasian surface T anomaly after splits	up to −3 K

Table 3a. SSW frequency by ENSO phase, 1958–2024 (67 winters; events: compendium + 2024×2). The ENSO phase is defined by ONI_DJF. The last column is not a chronological per-decade rate but the descriptive equivalent of the total number of events scaled to 10 winters by the number of phase-winters (events per 10 phase-winters).

Phase	No. of winters	Winters with ≥1 SSW	Events	Events per 10 phase-winters
El Niño	24	14 (58%)	19	7.9
La Niña	23	15 (65%)	17	7.4
Neutral	20	9 (45%)	11	5.5

Table 3b. Sensitivity of winter-based SSW risk to the QBO phase definition. Outcome: at least one major SSW within the winter. Intervals are Clopper–Pearson exact 95% intervals; the risk ratio interval is computed on the log scale and p is Fisher's exact test.

QBO definition	Period	eQBO: ≥1 SSW	wQBO: ≥1 SSW	Risk ratio (95% CI)	**Fisher *p***
50 hPa November (main)	1980–2024	12/19 = 63% [38–84]	13/26 = 50% [30–70]	1.26 (0.75–2.12)	0.545
50 hPa November–December	1980–2024	12/19 = 63%	13/26 = 50%	1.26 (0.75–2.12)	0.545
50 hPa DJF (upper bound)	1980–2024	15/21 = 71%	10/24 = 42%	1.71 (0.99–2.96)	0.071
30 hPa November	1980–2024	16/25 = 64%	9/20 = 45%	1.42 (0.81–2.51)	0.239
30 hPa November (long record)	1958–2024	24/36 = 67% [49–81]	14/31 = 45% [27–64]	1.48 (0.94–2.32)	0.089

Table 3c. ENSO × QBO cells, winter-based risk (QBO phase = November 50 hPa; 1980–2024). Intervals are Clopper–Pearson exact; the last column is not a chronological time rate but the complementary event density scaled per 10 phase-winters.

Cell	Winter	≥1 SSW	Rate	95% exact CI	Events	Events per 10 phase-winters
La Niña × eQBO	6	5	0.83	0.36–1.00	6	10.0
La Niña × wQBO	10	7	0.70	0.35–0.93	7	7.0
Neutral × eQBO	7	4	0.57	0.18–0.90	5	7.1
Neutral × wQBO	6	1	0.17	0.00–0.64	2	3.3
El Niño × eQBO	6	3	0.50	0.12–0.88	4	6.7

Cell	Winter	≥1 SSW	Rate	95% exact CI	Events	Events per 10 phase-winters
El Niño × wQBO	10	5	0.50	0.19–0.81	7	7.0

Stratified Fisher's exact tests: La Niña p=1.000; neutral p=0.266 (odds ratio 6.67); El Niño p=1.000 (odds ratio 1.00). Firth penalized logistic model (ssw ~ eQBO + El Niño + eQBO×El Niño; n=45): odds ratio 2.11 for eQBO (95% CI 0.46–9.67) and 0.47 for the interaction (0.04–5.96), with a profile penalized LRT p=0.541. When the same model is built with the 30-hPa November phase and the 1958–2024 record (n=67), the collapse in the El Niño cells disappears (eQBO 9/13 = 0.69; wQBO 5/11 = 0.45) and the interaction odds ratio returns to 1.13 (0.14–8.92; p=0.904): the interaction cannot be resolved with the present sample.

Acknowledgments

This research received no funding from any agency in the public, commercial or not-for-profit sectors. The author declares no conflicts of interest. The author thanks Prof. Dr. Mikdat Kadıoğlu (Department of Meteorological Engineering, Istanbul Technical University) for a detailed critical reading of the preprint version, which prompted the reframing of the problem in section 1, the literature additions in sections 3 and 5, and the power discussion in section 4, and acknowledges NOAA CPC, NOAA PSL, NOAA CSL and ECMWF for making the index series, reanalysis fields and event catalogs used here publicly available.

Data Availability Statement

All series used are publicly available: ONI and RONI (NOAA CPC, ERSSTv6), the monthly NAO and AO indices (CPC), the 50-hPa equatorial zonal wind (CPC/CDAS), the 30-hPa QBO series (NOAA PSL), the 10-hPa 60°N zonal-mean wind (NCEP/NCAR Reanalysis-1; NOAA PSL) and the major-SSW event catalog (NOAA CSL SSW Compendium; Butler et al. 2017), with Lee (2025) for the 2023/24 events. The monthly Z500, total precipitation and 2-m temperature fields used in the regional analysis are taken from the 1.5° monthly derivative of ERA5 distributed through the WeatherBench2 channel (Hersbach et al. 2020; Rasp et al. 2024); these fields were accessed on 29 August 2026 and all other series on 28 August 2026. The winter-based catalog, the derived frequency tables, the bootstrap/Fisher/Firth calculations and all scripts producing Figures 7–9 and Figure C1 have been prepared for publication in a permanent archive together with data access dates and version identifiers; the archive will be published on Zenodo before submission and the DOI entered in this statement (Zenodo DOI: reservation pending; version v1.1, 2026). The repository is prepared to contain not only the code but access-dated snapshots of the downloaded ONI, RONI, NAO, AO, QBO, SSW and ERA5 files, product version identifiers and a step-by-step reproduction guide in the README; Tables 1, 2a, 3a–3c, Appendices A/B, Appendix C (including Table C3) and the Appendix D likelihood ratios can all be reproduced from the raw series and fields. The decision rules of section 8.3 and Appendix D will be deposited separately, with a timestamp and before the start of the 2026/27 winter, in the Open Science Framework registry (OSF registration: pending).

Appendix A — Sensitivity to Threshold, Index and Definition

Table A1. Sensitivity of the super–wQBO pattern to the ONI threshold (1951–2024 catalog). The QBO phase is constructed with the main definition of the paper, the sign of the 50-hPa November mean; for winters before 1979 (1957/58, 1972/73) the CPC 50-hPa series is unavailable, so the phase is derived from the 30-hPa November mean and marked with ‡ in the table. SSW = at least one major event within the winter.

Threshold (ONI_DJF)	No. of winters	**wQBO**	**eQBO**	Winters with an SSW	Pattern
≥ +1.5	7	4	3	1957/58 (W‡), 1972/73 (E‡), 2023/24 (E)	mixed
≥ +1.8	4	3	1	2023/24 (E)	all wQBO winters SSW-free
≥ +2.0	3	3	0	—	pure: 3/3 wQBO and SSW-free

Reading: the pure form of the pattern appears only at the ≥+2.0 threshold; when the threshold is lowered to +1.5, both the strong easterly-QBO winters (1972/73 and 2023/24, each with an SSW) and 1957/58, which produced an SSW under westerly QBO, enter the table and the pattern becomes mixed. Because the threshold table uses the main phase definition, it is directly comparable with the 50-hPa November and 30-hPa November rows of Table A3. This sensitivity independently justifies keeping the proposition of section 5 at the status of a hypothesis.

Table A2. Comparison of the ONI and RONI rulers (winters satisfying ONI_DJF ≥ +1.5 or RONI_DJF ≥ +1.5; RONI: CPC relative ONI, accessed 28 Aug 2026).

Winter	**ONI (DJF)**	**RONI (DJF)**	QBO50 (Nov)	QBO30 (Nov)	Major midwinter SSW
1957/58	+1.7	+1.89	—	W	Yes
1965/66	+1.2	+1.53	—	E	Yes
1972/73	+1.6	+1.69	—	E	Yes
1982/83	+2.1	+2.40	W	W	No
1991/92	+1.5	+2.12	E	E	No
1997/98	+2.2	+2.13	W	W	No
2015/16	+2.5	+2.14	W	W	No
2023/24	+1.8	+1.13	E	E	Yes (two events)

Reading: the RONI≥+2.0 set comprises four winters, all four free of a major midwinter SSW, so the change of ruler extends the SSW-free component from 3/3 to 4/4. Phase purity weakens instead: 1991/92 is eQBO and the wQBO share falls to 3/4. The SSW-free pattern and the wQBO conditioning hypothesis are thus not equally robust to a change of index. While 2023/24 approaches the super threshold in ONI, it falls back markedly in RONI.

Table A3. Sensitivity of the super–wQBO pattern to the QBO phase definition. Each cell gives, in order, the number of westerly-QBO winters, the number of easterly-QBO winters, and the number of winters with at least one major SSW among the winters satisfying the corresponding ONI threshold; the sum of the first two numbers equals the number of winters that can be classified at that threshold.

QBO definition	**ONI ≥ +2.0 (n=3)**	**ONI ≥ +1.8 (n=4)**	**ONI ≥ +1.5 (n=7)**
50 hPa November	3 / 0 / 0	3 / 1 / 1	3 / 2 / 3 (two winters unclassifiable†)
50 hPa November–December	3 / 0 / 0	3 / 1 / 1	3 / 2 / 3 (two winters unclassifiable†)
50 hPa DJF	3 / 0 / 0	3 / 1 / 1	3 / 2 / 3 (two winters unclassifiable†)
30 hPa November	3 / 0 / 0	3 / 1 / 1	4 / 3 / 3
30 hPa DJF	2 / 1 / 0	2 / 2 / 1	3 / 4 / 3

† For 1957/58 and 1972/73 the CPC 50-hPa series does not extend before 1979, so these two winters can be classified only in the 30-hPa rows.

Reading: at the ONI ≥ +2.0 threshold the 3/3 westerly-QBO pattern is preserved in the three 50-hPa windows and under 30-hPa November; only the 30-hPa DJF definition moves 1997/98 to the easterly side. When the threshold is lowered to +1.5 the pattern becomes mixed under every definition.

Appendix B — Split/Displacement Surface Composites

Table B1. Surface signatures compiled from the literature (to be read together with the caveats discussed in section 6).

Surface signature	Split (S)	Displacement (D)	Source
Eurasian surface temperature	cooling of up to −3 K	markedly weaker	Mitchell et al. (2013)
Eastern North America	warming exceeding +1.5 K	cooling of about −1.5 K	Mitchell et al. (2013)
Timing of surface descent	about 1 week earlier; immediate and barotropic	lagged by 1–2 weeks	Seviour et al. (2013); Hall et al. (2021); White et al. (2021)
NAO/NAM signature difference	small	small	Hall et al. (2021)
After 3–4 weeks	no difference	no difference	White et al. (2021); Maycock and Hitchcock (2015)
Statistical status	significant in reanalysis, not in large ensembles	—	Charlton and Polvani (2007); Lehtonen and Karpechko (2016); White et al. (2019)

Appendix C — Details of the Vortex–Türkiye Regression (ERA5)

This appendix gives the full coefficient table of the ERA5 regional regression summarized in section 7.1 together with the ND/JFM maps. The design, data and uncertainty method are defined in section 2.2; in all five boxes the area mean is cosine-latitude weighted and taken without a land–sea mask, all values are per +1 standard deviation of DJF U10–60N, and the signs reverse symmetrically for weak-vortex winters.

Table C1. Grid-level significance summary: fraction of grid cells with local $p<0.05$, fraction passing BH-FDR ($\alpha=0.10$), and the correlation of the DJF-predictor pattern with the concurrent-predictor pattern (conc_r; an indicator of acausality for ND).

Window	Variable	Local % <0.05	% passing FDR	**conc_r**
DJF	Z500	42.0	36.6	1.00
DJF	Precipitation	12.4	1.5	1.00
DJF	T2m	17.9	2.0	1.00
ND	Z500	18.8	16.6	0.68
ND	Precipitation	7.9	0.0	0.55
ND	T2m	10.7	0.0	0.47
JFM	Z500	34.6	25.4	0.96
JFM	Precipitation	10.9	1.0	0.90
JFM	T2m	19.0	6.5	0.91

Table C2. Regional mean precipitation coefficients (mm month^{-1} per +1 sd U10–60N; winter-based bootstrap 95% CI); the regional means are cosine-latitude-weighted full-area means taken without a land–sea mask. Model A: U10 only; Model B: U10 + concurrent NAO; Indirect = bootstrap distribution of the A − B difference. Concurrent U10–NAO correlation: DJF r=+0.41, ND +0.10, JFM +0.45.

Window	Region	Model A β [95% CI]	% clim.	**Model B β**	Indirect (A−B) [95% CI]
DJF	Türkiye	−5.49 [−10.24, −0.62]	−6.8	−5.28	−0.17 [−2.37, +1.75]
DJF	Marmara	−5.46 [−10.55, −0.39]	−6.9	−4.61	−0.70 [−4.57, +2.18]
DJF	Aegean	−9.69 [−17.26, −1.87]	−10.0	−8.50	−1.00 [−6.16, +3.29]
DJF	Mediterranean coast	−8.79 [−18.94, +1.69]	−8.1	−8.97	+0.15 [−3.72, +4.70]
DJF	Levant	−2.79 [−8.54, +2.98]	−4.0	−3.13	+0.28 [−1.36, +2.57]
ND	Türkiye	−4.28 [−10.89, +2.10]	−5.7	−4.00	−0.18 [−2.39, +0.73]
ND	Marmara	−3.50 [−12.54, +5.88]	−4.4	−2.71	−0.66 [−3.98, +1.59]
ND	Aegean	−4.27 [−15.28, +5.87]	−4.8	−3.12	−1.07 [−5.80, +2.17]
ND	Mediterranean coast	−11.89 [−24.43, −0.56]	−12.1	−10.95	−0.78 [−5.01, +1.79]
ND	Levant	−6.55 [−12.46, −0.50]	−11.1	−6.51	−0.02 [−1.15, +0.75]
JFM	Türkiye	−2.25 [−6.35, +1.61]	−2.9	+0.10	−2.17 [−5.62, −0.04]
JFM	Marmara	−3.26 [−8.28, +1.39]	−4.5	+1.04	−4.07 [−8.59, −0.85]
JFM	Aegean	−5.72 [−12.50, +0.84]	−6.5	−1.82	−3.66 [−9.57, +0.15]
JFM	Mediterranean coast	−2.41 [−10.16, +5.13]	−2.7	−0.43	−1.76 [−7.97, +2.57]
JFM	Levant	−0.27 [−4.74, +3.92]	−0.5	−0.28	+0.02 [−2.80, +2.66]

Reading: in the DJF rows all five regions give negative coefficients and three exclude zero; in ND the signal shifts to the southern coastal belt; in JFM all intervals include zero and, while controlling for the NAO erases the coefficients, the indirect component moves away from zero. The ND rows should be read more cautiously because of the partial acausality of the DJF predictor with respect to the ND response (conc_r=0.68 in Table C1). When the fifteen Model-A coefficients are treated as a single family under BH-FDR (α=0.10), none passes the threshold (smallest p=0.022, DJF Türkiye box); individual intervals that exclude zero are exploratory signals.

Table C3. Sensitivity of the box means to the land–sea mask: the Model-A coefficients of Table C2 repeated with cosine-latitude-weighted land-cell means of the same five boxes restricted by the ERA5 land–sea mask (land fraction ≥0.5) (mm month^{-1} per +1 sd U10–60N; winter-based bootstrap, B=5000, 95% percentile CI). The full-area coefficients are identical to Table C2, and the land-masked intervals were produced with the same bootstrap design and seed as Table C2.

Window	Region	Full-area β (Table C2)	Land-masked β [95% CI]	**% clim. (land)**	Land cells / total
DJF	Türkiye	−5.49	−5.55 [−9.98, −0.95]	−7.3	49 / 65
DJF	Marmara	−5.46	−5.64 [−11.03, −0.16]	−6.9	4 / 6
DJF	Aegean	−9.69	−9.10 [−15.84, −2.10]	−10.1	5 / 6
DJF	Mediterranean coast	−8.79	−8.06 [−16.64, +0.73]	−8.4	6 / 10
DJF	Levant	−2.79	−3.82 [−8.31, +0.85]	−5.5	6 / 32
ND	Türkiye	−4.28	−3.54 [−9.64, +2.51]	−4.9	49 / 65
ND	Marmara	−3.50	−3.23 [−12.63, +6.37]	−3.9	4 / 6
ND	Aegean	−4.27	−3.24 [−14.30, +6.73]	−3.8	5 / 6
ND	Mediterranean coast	−11.89	−7.49 [−18.17, +2.39]	−8.7	6 / 10
ND	Levant	−6.55	−4.24 [−8.97, +0.69]	−7.7	6 / 32
JFM	Türkiye	−2.25	−2.22 [−6.31, +1.61]	−2.9	49 / 65
JFM	Marmara	−3.26	−3.31 [−8.76, +1.79]	−4.4	4 / 6
JFM	Aegean	−5.72	−5.25 [−11.72, +1.13]	−6.3	5 / 6
JFM	Mediterranean coast	−2.41	−2.03 [−8.94, +4.52]	−2.3	6 / 10
JFM	Levant	−0.27	−1.21 [−5.41, +2.79]	−1.9	6 / 32

Reading: in DJF the coefficients of the five regions change by about 1 mm month^{-1} under masking and the Türkiye, Marmara and Aegean intervals remain off zero; the land-masked DJF coefficient for the Levant grows but its interval continues to include zero. In ND the southern-coast signal weakens markedly and both intervals include zero; the “southward shift” of section 7.1 is therefore carried partly by sea cells. In JFM all intervals include zero under both conventions. At 1.5° the Marmara box under the mask consists of four land cells, the Aegean of five, and the Mediterranean coast and the Levant of six; this repetition does not substitute for station-scale verification.

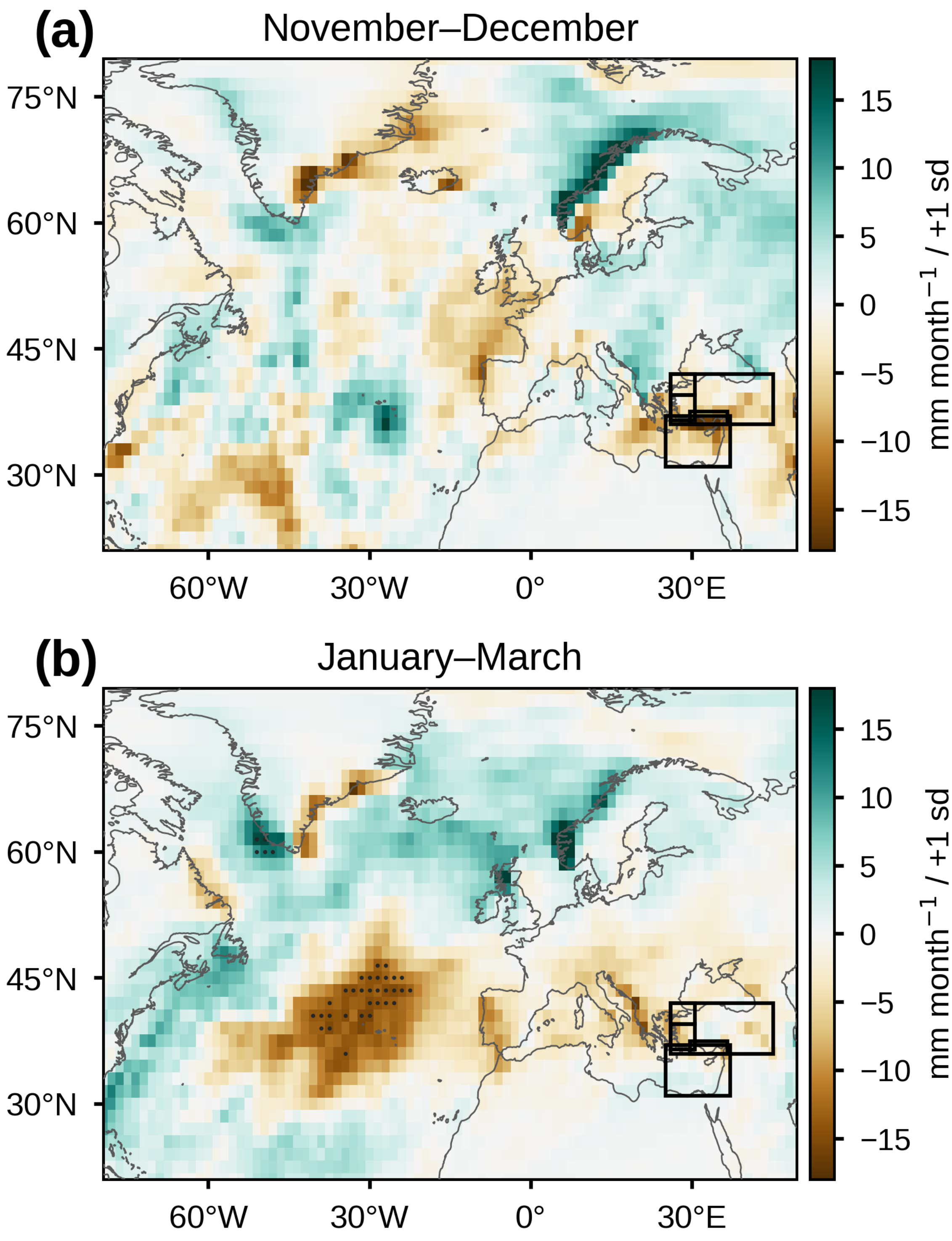

Figure C1. The ND (top) and JFM (bottom) counterparts of Figure 9: precipitation coefficient maps (mm month^{-1} per +1 sd DJF U10–60N) and the regional boxes; the stippling follows the same criterion as in Figure 9, and the boxes are full-area means without a land–sea mask. The ND panels are built with the DJF predictor and are partly acausal (pattern correlation with the concurrent predictor 0.68); in the JFM panel no regional interval excludes zero. The data identification is the same as in Figure 9. Quantitative figure.

Appendix D — Prospectively Defined Protocol for 2026/27

This appendix fixes the operational definitions of the discriminating observations of section 8.3 before the outcome of the winter is known and in a form that cannot be changed. Its purpose is to reduce the sensitivity ladder described in section 2.2 (more than one QBO level, month, ONI threshold and window) to a single path in the end-of-winter assessment; every calculation outside the definitions below will be counted as exploratory and labeled as such. The protocol will be deposited verbatim in a timestamped registry (OSF) before journal submission, and the registration identifier will be entered in this appendix.

The ENSO state is defined by the 2026/27 DJF value of NOAA CPC's ERSSTv6-based ONI series; the "super" threshold is ONI_DJF ≥ +2.0 °C. RONI is reported in parallel only for the ruler sensitivity of Table A2 and is not used for the super label. For the event-flavor candidate H4, the difference between the Niño-3 and Niño-4 DJF anomalies (ERSSTv6, CPC) is recorded; a Niño-4 anomaly exceeding Niño-3 assigns the label "Central-Pacific-weighted".

The QBO phase is the sign of the November 2026 monthly mean of the CPC/CDAS 50-hPa equatorial zonal-mean wind (main definition; first row of Table 3b). If $|u| < 1$ m s^{-1} the winter is labeled "transitional" and excluded from the main analysis; in that case the 30-hPa November sign is reported only as a sensitivity row. The November–December and DJF means will also be computed but will not be used in the evidence update; the risk ratio based on the DJF 50-hPa definition (1.71) enters no update because it overlaps the outcome period.

An SSW is, by the criterion of Charlton and Polvani (2007), a reversal to easterlies of the daily-mean 10-hPa 60°N zonal-mean zonal wind between November 2026 and March 2027; the outcome is at least one major event within the winter. The central date of the event is derived from ERA5 daily fields; if it disagrees with a label that the NOAA CSL Compendium may publish later, the ERA5 derivation is taken as the reference and the difference is reported. The split/displacement type is recorded but not used in the update.

The continuous vortex measure is the DJF mean U10–60N. For comparability with Table 1 the NCEP/NCAR Reanalysis-1 value is reported; the ERA5 (1940–2027) derivative is computed with the same definition and the two products are given side by side. If the ERA5 re-derivation planned for completion before submission (section 2.1) has been finished, Table 1, Table 2a and Figure 7 will have been repeated with ERA5 and the super-winter percentiles will be reported with that product. "Close to the historical super-winter range" is defined as the 2026/27 DJF U10–60N falling within the 20th–97th percentile band of the 1959–2024 distribution (the band spanned by the three super winters in Table 1).

The evidence update is made with likelihood ratios, and the ratios are fixed now. For H2 (QBO conditioning) the comparison is between the conditional proportions in the main row of Table 3b and the unconditional El Niño base rate of Table 3a (58%): if an SSW is observed under westerly QBO the likelihood ratio is 0.50/0.58 = 0.86, if none is observed 0.50/0.42 = 1.19; under easterly QBO the ratio is 0.63/0.58 = 1.09 if an SSW is observed and 0.37/0.42 = 0.88 if not. None of these ratios is more than 0.2 away from 1; a single winter neither confirms nor refutes any hypothesis but moves the relative weight by this much. For H1 the update is made only with the continuous measure: U10–60N falling within the band above despite record ENSO amplitude is recorded as "compatible" with the simple plateau expectation, and falling below the band as "less compatible"; because planetary-wave forcing is not measured directly, no mechanistic judgment is made about H1. No separate update is made for H3; H3 carries the weight that H1 and H2 do not gain. For H4 the Central Pacific label and the vortex outcome are recorded together; if 2026/27 turns out Eastern-Pacific-weighted, H4 is uninformative for this winter.

For the regional layer, the expected precipitation anomaly will be computed from the DJF Türkiye-box coefficient of Table C2 (−5.49 mm month^{-1} per +1 sd) and the standardized 2026/27 DJF U10–60N value, and compared with the realized ERA5 DJF anomaly in the same box and convention (cosine-latitude-weighted, unmasked; land-masked in parallel). This single-winter comparison is a case study and does not substitute for the long-record and large-ensemble arm of the main study.

The assessment calendar and freezing rule are as follows: the QBO phase is locked in the first week of December 2026 when the CPC November value is published, the SSW outcome on 1 April 2027, and ONI_DJF and U10–60N when the March 2027 data close. No definition will be changed after these dates; if any item of the protocol proves inapplicable, that fact and its reason will be reported and any alternative calculation given as exploratory under a separate heading.

Reproducibility Correction

During the reproducibility audit we determined that the regional box-average convention had been described incorrectly in the methods text. The printed coefficients were verified to have been produced from cosine-latitude-weighted full-area means without a land–sea mask, and the description of the method (sections 2.2 and 9 and Appendix C) was corrected accordingly. In the same audit the bootstrap intervals of Table C2 were found not to be reproducible from the archived script; the fifteen Model-A intervals and the fifteen indirect-component intervals were rewritten from a fixed-seed run of the script (seed 42), and all interval references in the text and Figure 9d were updated accordingly; the point estimates, climatology percentages, grid-level FDR fractions and no qualitative result changed.

Use of Generative AI Tools

Generative artificial intelligence tools were used as an auxiliary aid in the conceptual visualization of the study and the development of the figure design, in cross-checking code and calculations, and in verifying table–text consistency. Figures 1–6 are conceptual drawings reconstructed in vector form and are not quantitative data maps; Figures 7–9 and Figure C1 were produced directly from data series and fields. All numerical results were computed from publicly available data series with the scripts published in the supplement, and AI outputs were not used as independent data or as scientific evidence.

References

Afargan-Gerstman, H., and D. I. V. Domeisen, 2020: Pacific modulation of the North Atlantic storm track response to sudden stratospheric warming events. Geophys. Res. Lett., 47, e2019GL085007, doi:10.1029/2019GL085007.

Anstey, J. A., and T. G. Shepherd, 2014: High-latitude influence of the quasi-biennial oscillation. Quart. J. Roy. Meteor. Soc., 140, 1–21, doi:10.1002/qj.2132.

Ayarzagüena, B., S. Ineson, N. J. Dunstone, M. P. Baldwin, and A. A. Scaife, 2018: Intraseasonal effects of El Niño–Southern Oscillation on North Atlantic climate. J. Climate, 31, 8861–8873, doi:10.1175/JCLI-D-18-0097.1.

Baldwin, M. P., and T. J. Dunkerton, 2001: Stratospheric harbingers of anomalous weather regimes. Science, 294, 581–584, doi:10.1126/science.1063315.

Baldwin, M. P., and Coauthors, 2021: Sudden stratospheric warmings. Rev. Geophys., 59, e2020RG000708, doi:10.1029/2020RG000708.

Baltacı, H., B. O. Akkoyunlu, and M. Tayanç, 2018: Relationships between teleconnection patterns and Turkish climatic extremes. Theor. Appl. Climatol., 134, 1365–1386, doi:10.1007/s00704-017-2350-z.

Barriopedro, D., and N. Calvo, 2014: On the relationship between ENSO, stratospheric sudden warmings, and blocking. J. Climate, 27, 4704–4720, doi:10.1175/jcli-d-13-00770.1.

Barton, C. A., and J. P. McCormack, 2017: Origin of the 2016 QBO disruption and its relationship to extreme El Niño events. Geophys. Res. Lett., 44, 11 150–11 157, doi:10.1002/2017GL075576.

Bell, C. J., L. J. Gray, A. J. Charlton-Perez, M. M. Joshi, and A. A. Scaife, 2009: Stratospheric communication of El Niño teleconnections to European winter. J. Climate, 22, 4083–4096, doi:10.1175/2009jcli2717.1.

Benjamini, Y., and Y. Hochberg, 1995: Controlling the false discovery rate: A practical and powerful approach to multiple testing. J. Roy. Statist. Soc., 57B, 289–300.

Butler, A. H., and L. M. Polvani, 2011: El Niño, La Niña, and stratospheric sudden warmings: A reevaluation in light of the observational record. Geophys. Res. Lett., 38, L13807, doi:10.1029/2011GL048084.

Butler, A. H., D. J. Seidel, S. C. Hardiman, N. Butchart, T. Birner, and A. Match, 2015: Defining sudden stratospheric warmings. Bull. Amer. Meteor. Soc., 96, 1913–1928, doi:10.1175/bams-d-13-00173.1.

Butler, A. H., J. P. Sjoberg, D. J. Seidel, and K. H. Rosenlof, 2017: A sudden stratospheric warming compendium. Earth Syst. Sci. Data, 9, 63–76, doi:10.5194/essd-9-63-2017.

Cagnazzo, C., and E. Manzini, 2009: Impact of the stratosphere on the winter tropospheric teleconnections between ENSO and the North Atlantic and European region. J. Climate, 22, 1223–1238, doi:10.1175/2008jcli2549.1.

Calvo, N., M. A. Giorgetta, R. Garcia-Herrera, and E. Manzini, 2009: Nonlinearity of the combined warm ENSO and QBO effects on the Northern Hemisphere polar vortex in MAECHAM5 simulations. J. Geophys. Res., 114, D13109, doi:10.1029/2008jd011445.

Charlton, A. J., and L. M. Polvani, 2007: A new look at stratospheric sudden warmings. Part I: Climatology and modeling benchmarks. J. Climate, 20, 449–469, doi:10.1175/jcli3996.1.

Coy, L., P. A. Newman, S. Pawson, and L. R. Lait, 2017: Dynamics of the disrupted 2015/16 quasi-biennial oscillation. J. Climate, 30, 5661–5674, doi:10.1175/jcli-d-16-0663.1.

Domeisen, D. I. V., C. I. Garfinkel, and A. H. Butler, 2019: The teleconnection of El Niño Southern Oscillation to the stratosphere. Rev. Geophys., 57, 5–47, doi:10.1029/2018rg000596.

Dunkerton, T. J., D. P. Delisi, and M. P. Baldwin, 1988: Distribution of major stratospheric warmings in relation to the quasi-biennial oscillation. Geophys. Res. Lett., 15, 136–139, doi:10.1029/gl015i002p00136.

Ebdon, R. A., 1975: The quasi-biennial oscillation and its association with tropospheric circulation patterns. Meteor. Mag., 104, 282–297.

Garfinkel, C. I., and D. L. Hartmann, 2008: Different ENSO teleconnections and their effects on the stratospheric polar vortex. J. Geophys. Res., 113, D18114, doi:10.1029/2008jd009920.

Garfinkel, C. I., A. H. Butler, D. W. Waugh, M. M. Hurwitz, and L. M. Polvani, 2012a: Why might stratospheric sudden warmings occur with similar frequency in El Niño and La Niña winters? J. Geophys. Res., 117, D19106, doi:10.1029/2012JD017777.

Garfinkel, C. I., T. A. Shaw, D. L. Hartmann, and D. W. Waugh, 2012b: Does the Holton–Tan mechanism explain how the quasi-biennial oscillation modulates the Arctic polar vortex? J. Atmos. Sci., 69, 1713–1733, doi:10.1175/JAS-D-11-0209.1.

Garfinkel, C. I., M. M. Hurwitz, D. W. Waugh, and A. H. Butler, 2013: Are the teleconnections of Central Pacific and Eastern Pacific El Niño distinct in boreal wintertime? Climate Dyn., 41, 1835–1852, doi:10.1007/s00382-012-1570-2.

Geng, X., W. Zhang, M. F. Stuecker, and F.-F. Jin, 2017: Strong sub-seasonal wintertime cooling over East Asia and Northern Europe associated with super El Niño events. Sci. Rep., 7, 3770, doi:10.1038/s41598-017-03977-2.

Gray, L. J., J. A. Anstey, Y. Kawatani, H. Lu, S. Osprey, and V. Schenzinger, 2018: Surface impacts of the quasi biennial oscillation. Atmos. Chem. Phys., 18, 8227–8247, doi:10.5194/acp-18-8227-2018.

Hall, R. J., D. M. Mitchell, W. J. M. Seviour, and C. J. Wright, 2021: Tracking the stratosphere-to-surface impact of sudden stratospheric warmings. J. Geophys.

Res. Atmos., 126, e2020JD033881, doi:10.1029/2020jd033881.

Hardiman, S. C., N. J. Dunstone, A. A. Scaife, D. M. Smith, S. Ineson, J. Lim, and D. Fereday, 2019: The impact of strong El Niño and La Niña events on the North Atlantic. Geophys. Res. Lett., 46, 2874–2883, doi:10.1029/2018GL081776.

Hegyi, B. M., Y. Deng, R. X. Black, and R. Zhou, 2014: Initial transient response of the winter polar stratospheric vortex to idealized equatorial Pacific sea surface temperature anomalies in the NCAR WACCM. J. Climate, 27, 2699–2713, doi:10.1175/JCLI-D-13-00289.1.

Hersbach, H., and Coauthors, 2020: The ERA5 global reanalysis. Quart. J. Roy. Meteor. Soc., 146, 1999–2049, doi:10.1002/qj.3803.

Holton, J. R., and H.-C. Tan, 1980: The influence of the equatorial quasi-biennial oscillation on the global circulation at 50 mb. J. Atmos. Sci., 37, 2200–2208, doi:10.1175/1520-0469(1980)037<2200:tioteq>2.0.co;2.

Ineson, S., and A. A. Scaife, 2009: The role of the stratosphere in the European climate response to El Niño. Nat. Geosci., 2, 32–36, doi:10.1038/ngeo381.

Iza, M., and N. Calvo, 2015: Role of stratospheric sudden warmings on the response to Central Pacific El Niño. Geophys. Res. Lett., 42, 2482–2489, doi:10.1002/2014GL062935.

Jiménez-Esteve, B., and D. I. V. Domeisen, 2020: Nonlinearity in the tropospheric pathway of ENSO to the North Atlantic. Wea. Climate Dyn., 1, 225–245, doi:10.5194/wcd-1-225-2020.

Johnson, S. J., and Coauthors, 2019: SEAS5: The new ECMWF seasonal forecast system. Geosci. Model Dev., 12, 1087–1117, doi:10.5194/gmd-12-1087-2019.

Kalnay, E., and Coauthors, 1996: The NCEP/NCAR 40-year reanalysis project. Bull. Amer. Meteor. Soc., 77, 437–471, doi:10.1175/1520-0477(1996)077<0437:TNYRP>2.0.CO;2.

Karpechko, A. Yu., P. Hitchcock, D. H. W. Peters, and A. Schneidereit, 2017: Predictability of downward propagation of major sudden stratospheric warmings. Quart. J. Roy. Meteor. Soc., 143, 1459–1470, doi:10.1002/qj.3017.

King, M. P., I. Herceg-Bulić, I. Bladé, J. García-Serrano, N. Keenlyside, F. Kucharski, C. Li, and S. Sobolowski, 2018: Importance of late fall ENSO teleconnection in the Euro-Atlantic sector. Bull. Amer. Meteor. Soc., 99, 1337–1343, doi:10.1175/BAMS-D-17-0020.1.

Kömüşcü, A. Ü., and K. Oğuz, 2021: Analysis of cold anomalies observed over Turkey during the 2018/2019 winter in relation to polar vortex and other atmospheric patterns. Meteor. Atmos. Phys., 133, 1327–1354, doi:10.1007/s00703-021-00806-0.

Kosaka, Y., and Coauthors, 2024: The JRA-3Q reanalysis. J. Meteor. Soc. Japan, 102, 49–109, doi:10.2151/jmsj.2024-004.

Krichak, S. O., P. Kishcha, and P. Alpert, 2002: Decadal trends of main Eurasian oscillations and the eastern Mediterranean precipitation. Theor. Appl. Climatol., 72, 209–220, doi:10.1007/s007040200021.

Kumar, V., S. Yoden, and M. H. Hitchman, 2022: QBO and ENSO effects on the mean meridional circulation, polar vortex, subtropical westerly jets, and wave patterns during boreal winter. J. Geophys. Res. Atmos., 127, e2022JD036691, doi:10.1029/2022jd036691.

Kutiel, H., and Y. Benaroch, 2002: North Sea–Caspian Pattern (NCP)—an upper level atmospheric teleconnection affecting the Eastern Mediterranean: Identification and definition. Theor. Appl. Climatol., 71, 17–28, doi:10.1007/s704-002-8205-x.

Lee, S. H., 2025: Two major sudden stratospheric warmings during winter 2023/2024. Weather, 80, 45–53, doi:10.1002/wea.7656.

Lehtonen, I., and A. Yu. Karpechko, 2016: Observed and modeled tropospheric cold anomalies associated with sudden stratospheric warmings. J. Geophys. Res. Atmos., 121, 1591–1610, doi:10.1002/2015JD023860.

Lu, H., M. H. Hitchman, L. J. Gray, J. A. Anstey, and S. M. Osprey, 2020: On the role of Rossby wave breaking in the quasi-biennial modulation of the stratospheric polar vortex during boreal winter. Quart. J. Roy. Meteor. Soc., 146, 1939–1959, doi:10.1002/qj.3775.

Manzini, E., M. A. Giorgetta, M. Esch, L. Kornblueh, and E. Roeckner, 2006: The influence of sea surface temperatures on the northern winter stratosphere: Ensemble simulations with the MAECHAM5 model. J. Climate, 19, 3863–3881, doi:10.1175/JCLI3826.1.

Manzini, E., and Coauthors, 2024: Nonlinearity and asymmetry of the ENSO stratospheric pathway to North Atlantic and Europe, revisited. J. Geophys. Res. Atmos., 129, e2023JD039992, doi:10.1029/2023jd039992.

Marshall, A. G., and A. A. Scaife, 2009: Impact of the QBO on surface winter climate. J. Geophys. Res., 114, D18110, doi:10.1029/2009jd011737.

Maycock, A. C., and P. Hitchcock, 2015: Do split and displacement sudden stratospheric warmings have different annular mode signatures? Geophys. Res. Lett., 42, 10943–10951, doi:10.1002/2015gl066754.

Mezzina, B., J. García-Serrano, I. Bladé, and F. Kucharski, 2020: Dynamics of the ENSO teleconnection and NAO variability in the North Atlantic–European late winter. J. Climate, 33, 907–923, doi:10.1175/JCLI-D-19-0192.1.

Mitchell, D. M., L. J. Gray, J. Anstey, M. P. Baldwin, and A. J. Charlton-Perez, 2013: The influence of stratospheric vortex displacements and splits on surface climate. J. Climate, 26, 2668–2682, doi:10.1175/jcli-d-12-00030.1.

Moron, V., and I. Gouirand, 2003: Seasonal modulation of the El Niño–Southern Oscillation relationship with sea level pressure anomalies over the North Atlantic in October–March 1873–1996. Int. J. Climatol., 23, 143–155, doi:10.1002/joc.868.

Nakagawa, K. I., and K. Yamazaki, 2006: What kind of stratospheric sudden warming propagates to the troposphere? Geophys. Res. Lett., 33, L04801, doi:10.1029/2005gl024784.

Newman, P. A., L. Coy, S. Pawson, and L. R. Lait, 2016: The anomalous change in the QBO in 2015–2016. Geophys. Res. Lett., 43, 8791–8797, doi:10.1002/2016gl070373.

Osprey, S. M., N. Butchart, J. R. Knight, A. A. Scaife, K. Hamilton, J. A. Anstey, V. Schenzinger, and C. Zhang, 2016: An unexpected disruption of the atmospheric quasi-biennial oscillation. Science, 353, 1424–1427, doi:10.1126/science.aah4156.

Paek, H., J.-Y. Yu, and C. Qian, 2017: Why were the 2015/2016 and 1997/1998 extreme El Niños different? Geophys. Res. Lett., 44, 1848–1856, doi:10.1002/2016GL071515.

Palmeiro, F. M., and Coauthors, 2023: On the influence of ENSO on sudden stratospheric warmings. J. Geophys. Res. Atmos., 128, e2022JD037607, doi:10.1029/2022jd037607.

Polvani, L. M., L. Sun, A. H. Butler, J. H. Richter, and C. Deser, 2017: Distinguishing stratospheric sudden warmings from ENSO as key drivers of wintertime climate variability over the North Atlantic and Eurasia. J. Climate, 30, 1959–1969, doi:10.1175/JCLI-D-16-0277.1.

Rao, J., and R. Ren, 2016a: Asymmetry and nonlinearity of the influence of ENSO on the northern winter stratosphere: 1. Observations. J. Geophys. Res. Atmos., 121, 9000–9016, doi:10.1002/2015JD024520.

Rao, J., and R. Ren, 2016b: Asymmetry and nonlinearity of the influence of ENSO on the northern winter stratosphere: 2. Model study with WACCM. J. Geophys. Res. Atmos., 121, 9017–9032, doi:10.1002/2015JD024521.

Rasp, S., and Coauthors, 2024: WeatherBench 2: A benchmark for the next generation of data-driven global weather models. J. Adv. Model. Earth Syst., 16, e2023MS004019, doi:10.1029/2023MS004019.

Ren, R.-C., and Coauthors, 2017: Parallel comparison of the 1982/83, 1997/98 and 2015/16 super El Niños and their effects on the extratropical stratosphere. Adv. Atmos. Sci., 34, 1121–1133, doi:10.1007/s00376-017-6260-x.

Richter, J. H., K. Matthes, N. Calvo, and L. J. Gray, 2011: Influence of the quasi-biennial oscillation and El Niño–Southern Oscillation on the frequency of sudden stratospheric warmings. J. Geophys. Res., 116, D20111, doi:10.1029/2011jd015757.

Scaife, A. A., and Coauthors, 2014: Skillful long-range prediction of European and North American winters. Geophys. Res. Lett., 41, 2514–2519, doi:10.1002/2014gl059637.

Seviour, W. J. M., D. M. Mitchell, and L. J. Gray, 2013: A practical method to identify displaced and split stratospheric polar vortex events. Geophys. Res. Lett., 40, 5268–5273, doi:10.1002/grl.50927.

Sezen, C., and T. Partal, 2019: The impacts of Arctic oscillation and the North Sea Caspian pattern on the temperature and precipitation regime in Turkey. Meteor. Atmos. Phys., 131, 1677–1696, doi:10.1007/s00703-019-00665-w.

Soci, C., H. Hersbach, A. Simmons, P. Poli, B. Bell, P. Berrisford, A. Horányi, J. Muñoz-Sabater, J. Nicolas, R. Radu, D. Schepers, A. Villaume, L. Bidlot, and D. Dee, 2024: The ERA5 global reanalysis from 1940 to 2022. Quart. J. Roy. Meteor. Soc., 150, 4014–4048, doi:10.1002/qj.4803.

Toniazzo, T., and A. A. Scaife, 2006: The influence of ENSO on winter North Atlantic climate. Geophys. Res. Lett., 33, L24704, doi:10.1029/2006GL027881.

Trascasa-Castro, P., A. C. Maycock, Y. Y. Scott Yiu, and J. K. Fletcher, 2019: On the linearity of the stratospheric and Euro-Atlantic sector response to ENSO. J. Climate, 32, 6607–6626, doi:10.1175/JCLI-D-18-0746.1.

Trigo, R. M., and Coauthors, 2006: Relations between variability in the Mediterranean region and mid-latitude variability. Mediterranean Climate Variability, P. Lionello et al., Eds., Elsevier, 179–226, doi:10.1016/s1571-9197(06)80006-6.

Türkeş, M., and E. Erlat, 2003: Precipitation changes and variability in Turkey linked to the North Atlantic Oscillation during the period 1930–2000. Int. J. Climatol., 23, 1771–1796, doi:10.1002/joc.962.

Türkeş, M., and E. Erlat, 2008: Influence of the Arctic Oscillation on variability of winter mean temperatures in Turkey. Theor. Appl. Climatol., 92, 75–85, doi:10.1007/s00704-007-0310-8.

Watson, P. A. G., and L. J. Gray, 2014: How does the quasi-biennial oscillation affect the stratospheric polar vortex? J. Atmos. Sci., 71, 391–409, doi:10.1175/jas-d-13-096.1.

Wei, K., W. Chen, and R. Huang, 2007: Association of tropical Pacific sea surface temperatures with the stratospheric Holton–Tan oscillation in the Northern Hemisphere winter. Geophys. Res. Lett., 34, L16814, doi:10.1029/2007gl030478.

White, I. P., and Coauthors, 2019: The downward influence of sudden stratospheric warmings: Association with tropospheric precursors. J. Climate, 32, 85–108, doi:10.1175/jcli-d-18-0053.1.

White, I. P., and Coauthors, 2021: The impact of split and displacement sudden stratospheric warmings on the troposphere. J. Geophys. Res. Atmos., 126, e2020JD033989, doi:10.1029/2020jd033989.

Wilks, D. S., 2016: “The stippling shows statistically significant grid points”: How research results are routinely overstated and overinterpreted, and what to do about it. Bull. Amer. Meteor. Soc., 97, 2263–2273, doi:10.1175/BAMS-D-15-00267.1.

Zhang, C., J. Zhang, X. Xia, and D. Li, 2024: Impact of Arctic stratospheric polar vortex on Mediterranean precipitation. J. Climate, 37, 4403–4419, doi:10.1175/JCLI-D-23-0469.1.

Zhou, X., Q. Chen, F. Xie, J. Li, M. Li, R. Ding, Y. Li, X. Xia, and Z. Cheng, 2019: Nonlinear response of the Northern Hemisphere stratospheric polar vortex to the Indo–Pacific warm pool (IPWP) Niño. Sci. Rep., 9, 13719, doi:10.1038/s41598-019-49449-7.